nature cell biology

Melanoma miRNA trafficking controls tumour primary niche formation

Shani Dror[1,13], Laureen Sander[2,13], Hila Schwartz[3], Danna Sheinboim[1], Aviv Barzilai[4], Yuval Dishon[1], Sebastien Apcher[5], Tamar Golan[1], Shoshana Greenberger[4], Iris Barshack[4], Hagar Malcov[1], Alona Zilberberg[1], Lotan Levin[1], Michelle Nessling[6], Yael Friedmann[7], Vivien Igras[8], Ohad Barzilay[9], Hananya Vaknine[10], Ronen Brenner[10], Assaf Zinger[11], Avi Schroeder[11], Pinchas Gonen[1], Mehdi Khaled[12], Neta Erez[3], Jörg D. Hoheisel[2] and Carmit Levy[1,14]

Melanoma originates in the epidermis and becomes metastatic after invasion into the dermis. Prior interactions between melanoma cells and dermis are poorly studied. Here, we show that melanoma cells directly affect the formation of the dermal tumour niche by microRNA trafficking before invasion. Melanocytes, cells of melanoma origin, are specialized in releasing pigment vesicles, termed melanosomes. In melanoma *in situ*, we found melanosome markers in distal fibroblasts before melanoma invasion. The melanosomes carry microRNAs into primary fibroblasts triggering changes, including increased proliferation, migration and pro-inflammatory gene expression, all known features of cancer-associated fibroblasts (CAFs). Specifically, melanosomal microRNA-211 directly targets *IGF2R* and leads to MAPK signalling activation, which reciprocally encourages melanoma growth. Melanosome release inhibitor prevented CAF formation. Since the first interaction of melanoma cells with blood vessels occurs in the dermis, our data suggest an opportunity to block melanoma invasion by preventing the formation of the dermal tumour niche.

Melanoma, a neoplasm of melanocyte origin, is the most aggressive and treatment-resistant of all human skin cancers and responsible for approximately 80% of skin cancer mortalities[1]. Melanocytes produce the pigment melanin, which is stored in melanosomes. Melanosomes are tissue-specific organelles[2] classified into two main maturation stages based on morphology and pigmentation level[3]. Immature (stages I and II) melanosomes, termed early melanosomes, lack pigment and are located in the central cytoplasm. Pre-mature and mature melanosomes (stages III and IV) are heavily pigmented and predominate at distal dendrites, the main site of their secretion[2]. In normal skin, melanosomes are transferred to adjacent keratinocytes in response to ultraviolet exposure[4,5]. Melanin protects keratinocytes against ultraviolet radiation[4]. Melanoma cells keep certain features of their cellular origin, including melanosome production and trafficking[6–8]. In patients, keratinocytes surrounding melanoma cells often exhibit an abnormal distribution of melanin[8]. It has been suggested that melanosomes contribute to melanoma drug resistance by exporting chemotherapeutic agents from the tumour cells[9]. Whether melanoma melanosomes have a role in promoting melanoma tumorigenesis is unknown.

MicroRNAs (miRNAs) are small noncoding RNAs that suppress gene expression[10]. miRNAs regulate many physiological and pathophysiological processes such as development, differentiation and cancer[10,11]. Altered expression of a single miRNA can cause complex phenotypic changes[12,13]. We have previously uncovered a central role of miRNAs in the normal[14] and malignant[12] phenotypes of the melanocyte lineage.

The primary stage of melanoma involves proliferation of melanocytes from the basal epidermis toward the upper epidermis[15], termed melanoma *in situ*. Later, melanoma cells invade the dermis, which consists of mesenchymal components, mainly fibroblasts[16]. Melanoma proliferation in the dermis is crucial for disease development as it

[1]Department of Human Genetics and Biochemistry, Sackler Faculty of Medicine, Tel Aviv University, Tel Aviv 69978, Israel. [2]Functional Genome Analysis, Deutsches Krebsforschungszentrum (DKFZ), Heidelberg 69120, Germany. [3]Department of Pathology, Sackler Faculty of Medicine, Tel Aviv University, Tel Aviv 69978, Israel. [4]Institute of Pathology, Sheba Medical Center, Tel Hashomer 52621, Israel. [5]Department of Immunology, Institut Gustave Roussy, Université Paris, 94805 Villejuif, France. [6]Imaging and Cytometry Core Facility, Unit for Electron Microscopy, Deutsches Krebsforschungszentrum (DKFZ), Heidelberg 69120, Germany. [7]The Bio-Imaging Unit, Hebrew University, Jerusalem 91904, Israel. [8]Cutaneous Biology Research Center, Department of Dermatology and MGH Cancer Center, Massachusetts General Hospital, Boston, Massachusetts 02114, USA. [9]Coller School of Management, Tel Aviv University, Tel Aviv 69978, Israel. [10]Institute of Pathology, E. Wolfson Medical Center, Holon 58100, Israel. [11]Department of Chemical Engineering, Technion—Israel Institute of Technology, Haifa 32000, Israel. [12]INSERM 1186, Gustave Roussy, Université Paris-Saclay, Villejuif 94805, France. [13]These authors contributed equally to this work. [14]Correspondence should be addressed to C.L. (e-mail: carmitlevy@post.tau.ac.il)

Received 15 July 2015; accepted 18 July 2016; published online 22 August 2016; DOI: 10.1038/ncb3399

enlarges the contact to blood vessels, allowing metastasis[15]. Cancer-associated fibroblasts (CAFs) are an activated sub-population of stromal fibroblasts that have acquired a modified phenotype[17]. CAFs have a prominent role in cancer development[18,19] from initiation[17], to primary and metastatic tumour progression[20–22]. Compared with primary fibroblasts, CAFs have increased rates of proliferation and ability to migrate[17], promote inflammation[23], angiogenesis and tumour growth[24,25], and express α-SMA[26]. Co-culture of fibroblasts with melanoma cells induces both melanoma cell growth[27] and pro-inflammatory gene expression in fibroblasts[28]. Fibroblasts are reprogrammed into CAFs by secreted factors including TGF-β, osteopontin and IL1-β[23,25,29]. It is mostly unknown, however, which cells secrete the ligands that contribute to CAF reprogramming. Expression of certain miRNAs was shown to reprogram fibroblasts into CAFs[30], but the mechanisms underlying miRNA regulation of the fibroblast phenotype remain unknown.

On the basis of melanoma patient specimen analysis, we hypothesized that melanoma cells communicate with fibroblasts in the microenvironment via melanosomes, resulting in CAF formation. Here, we show that melanoma cells release melanosomes that contain miRNAs, which are transferred into fibroblasts. Specifically, melanosomal miR-211 induces primary fibroblast reprogramming as demonstrated by elevation of the pro-inflammatory gene signature, cell proliferation and migration. Finally, we demonstrate that melanosomal miR-211 directly targets *IGF2R* and thus induces MAPK signalling.

RESULTS

Fibroblast aggregations at a distance from melanoma regions contain melanoma particles

Studies have shown that there is an aggregation of fibroblasts at melanoma sites and that these cells support melanoma cell growth[31,32]. Haematoxylin and eosin staining of normal skin and melanoma regions from patients revealed melanoma *in situ* associated with fibroplasia of the superficial dermis (Fig. 1a and Supplementary Fig. 1a–h). To further assess the relationship between melanoma cells and fibroblasts, we stained clinical sections with a melanoma (HMB-45[6]) and a fibroblast marker (FSP-1[33]). In normal skin, we observed melanocytes in the basal layer of the epidermis and only few fibroblasts in the dermis, as expected[16]. In the primary disease stage, fibroblasts accumulated in the dermis at a distance from melanoma cells (Fig. 1b and Supplementary Fig. 1a–h). As melanoma progresses and invades the dermis, fibroblasts surround melanoma cells and fill the dermis (Fig. 1b and Supplementary Fig. 2a–d), as expected[31,32]. These observations suggest that fibroblasts begin to aggregate in the dermis at early stages of melanoma initiation, before melanoma cells invade, and that there is a distal paracrine communication between melanoma cells and fibroblasts.

Enhanced magnification of immunostaining images of melanoma *in situ* revealed HMB-45 expression in fibroblasts (Fig. 1b), suggesting that melanoma cells release melanosomes into the dermis before melanoma cells invasion. To explore this idea, we stained clinical sections for secreted melanosome markers GPNMB[34] and DCT[2], and fibroblast marker FSP-1[33]. Remarkably, significant melanosome uptake by dermal fibroblasts was observed in primary melanoma stage (Fig. 1c and Supplementary Fig. 1e–h). We quantified the melanosomes internalized by fibroblasts (Supplementary Fig. 2e) and found 200–500 melanosomes per melanoma dermal fibroblast and about 100 per fibroblast in normal skin (Fig. 1d and Supplementary Fig. 2e). No evidence for macrophage presence was observed in the aggregation regions (Supplementary Fig. 2f); macrophages were observed around vessels, as expected at early disease stages[35]. Additionally, in the dermal regions of these samples, there was no staining for MITF or MLANA, which are routinely used for melanoma diagnosis (Supplementary Fig. 1e–h). We therefore hypothesized that melanoma cells communicate with fibroblasts via trafficking of melanosomes.

Transfer of melanoma melanosomes into fibroblasts leads to reprogramming

Melanosome trafficking from normal melanocytes and melanoma cells to keratinocytes has previously been described[7,8] whereas transfer to fibroblasts is poorly characterized. To investigate the latter, we first determined whether fibroblasts take up melanosomes. Transmission electron microscopy (TEM) demonstrated a clear melanosome uptake by fibroblasts treated with medium from melanoma MNT-1 culture (Fig. 2a). Similar to the known characteristics of melanosomes[3], TEM of isolated MNT-1 melanosomes showed bright, relatively spherical organelles ranging in diameter from 200 to 500 nm with an amorphous matrix (early melanosomes) and dark elliptically shaped vesicles (mature melanosomes) (Fig. 2b). There was significantly more tyrosinase activity, a melanosome-specific enzyme[6], in mature and pre-mature melanosome fractions than in the whole-cell lysate (Supplementary Fig. 3a). High tyrosinase levels were found in mature melanosomes and not in cytoplasmic fractions (Supplementary Fig. 3b). To ensure that the melanosomes were not contaminated with exosomes, MNT-1 exosomes were isolated (Supplementary Fig. 3c,d) and compared with melanosome fractions (Supplementary Fig. 3e). No exosome markers (alpha-enolase and CD63[36]) were detected in melanosome fractions, whereas melanosome markers (tyrosinase, DCT and GPNMB) were. Additionally, the melanosomes were not contaminated with mitochondria as the mitochondrial-specific NADH dehydrogenase gene[37] was not expressed (Supplementary Fig. 3f). Together, these results confirmed that the isolated vesicles were indeed melanosomes.

Primary dermal fibroblasts were incubated with isolated melanosomes for 48 h and subsequently immunostained with the melanosomal markers HMB-45 and GPNMB (Fig. 2c); as a positive control[7], keratinocytes were treated with melanosomes (Supplementary Fig. 3g). Both cell types became positive for melanosomal markers, confirming that fibroblasts take up melanosomes.

We next asked whether tumour-derived melanosomes functionally affect primary fibroblasts. A standard curve of melanosome amounts was generated (Supplementary Fig. 3h) that allowed the use of a physiological number (Fig. 1d). Unbiased messenger RNA profiling of melanosome-treated fibroblasts or untreated fibroblasts and functional gene set enrichment analysis, using Ingenuity Pathway Analysis (IPA), revealed the potential biological relevance of the most differentially expressed genes (Supplementary Table 1). Uptake of melanoma melanosomes by fibroblasts resulted in an increased expression of genes associated with proliferation and cell motility (Fig. 2d and Supplementary Table 2). An increase in actual fibroblast proliferation and migration following melanosome treatment was validated experimentally (Fig. 2e,f).

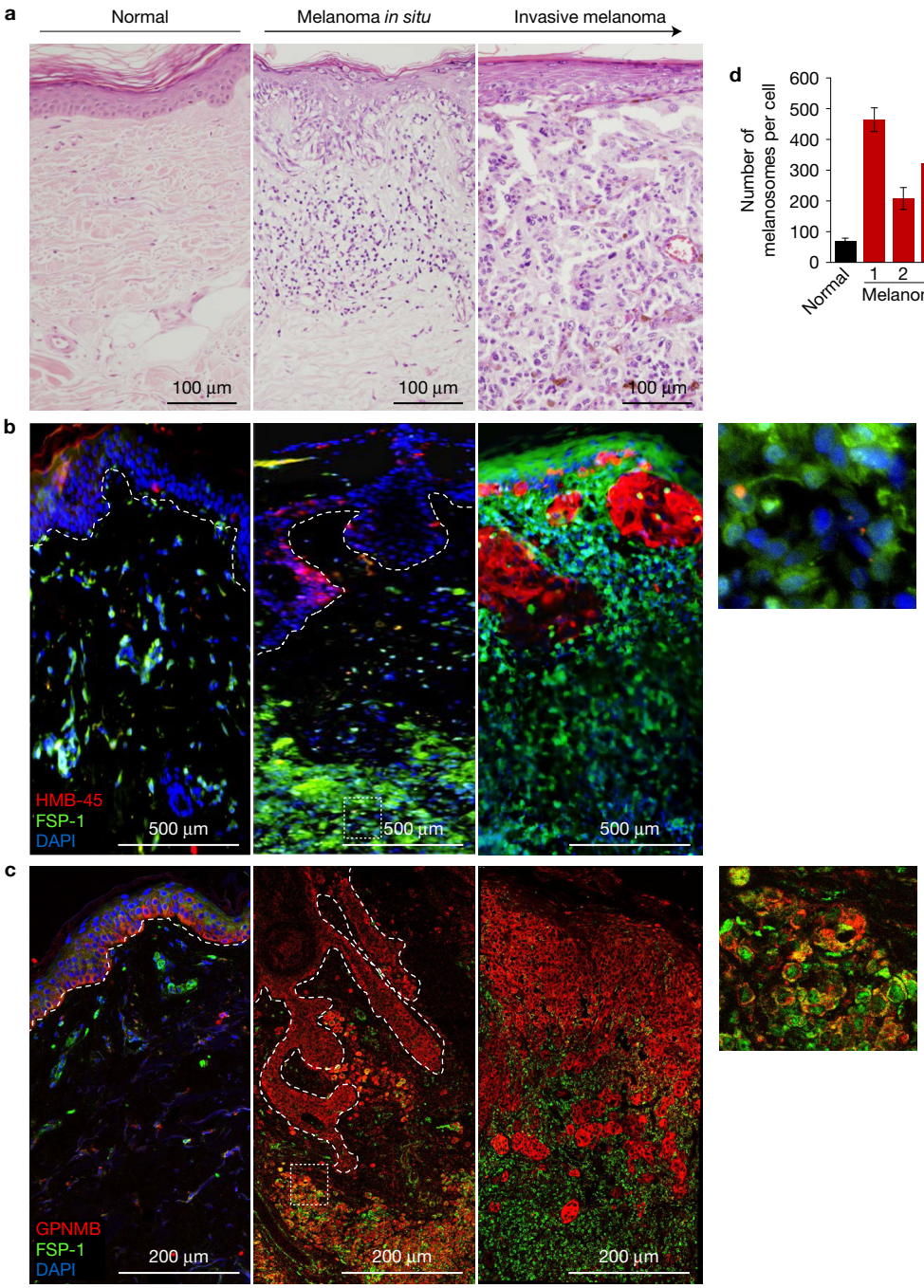

Figure 1 Fibroblast aggregations at a distance from melanoma regions contain melanoma particles. (**a**) Haematoxylin and eosin staining (×20 magnification) of typical vertical cross-sections made from one healthy skin sample (left) and two melanoma patient samples at different progression stages (right). (**b**,**c**) Immunofluorescence analysis (×20 magnification). DAPI-stained nuclei appear in blue. The white dashed lines represent the epidermal–dermal junction. (**b**) The melanoma tissues exhibit expression of the fibroblast marker FSP-1 (green) and the melanoma marker HMB-45 (red). At higher (×40) magnification of the area marked with a white dashed square, yellow signals indicate co-localization of HMB-45 and FSP-1 in the fibroblast congregation area. Each image was generated by merging of serial images (see Methods). (**c**) Similar sections stained with the fibroblast marker FSP-1 (green) and the secreted melanosome marker GPNMB (red). At higher (×63) magnification of the area marked with a white dashed square, yellow signals indicate co-localization of GPNMB and FSP-1 in the fibroblast congregation area. (**d**) Quantification of melanosomes (red fluorescence; see Methods) per dermal fibroblast in normal skin ($n = 30$ cells from one individual) and in three melanoma specimens ($n = 100$ cells from each patient 1, 2 and 3). In all relevant panels error bars represent ± s.e.m.

These changes led us to reason that melanoma melanosomes reprogram fibroblasts into CAFs[17]. CAFs have enhanced matrix adhesion abilities, leading to more contraction of collagen gel matrices in an integrin-dependent manner[38] and exhibit a pro-inflammatory gene signature[23–25]. As anticipated, melanosome treatment led to significant enhancement in collagen contraction (Fig. 2g) and a

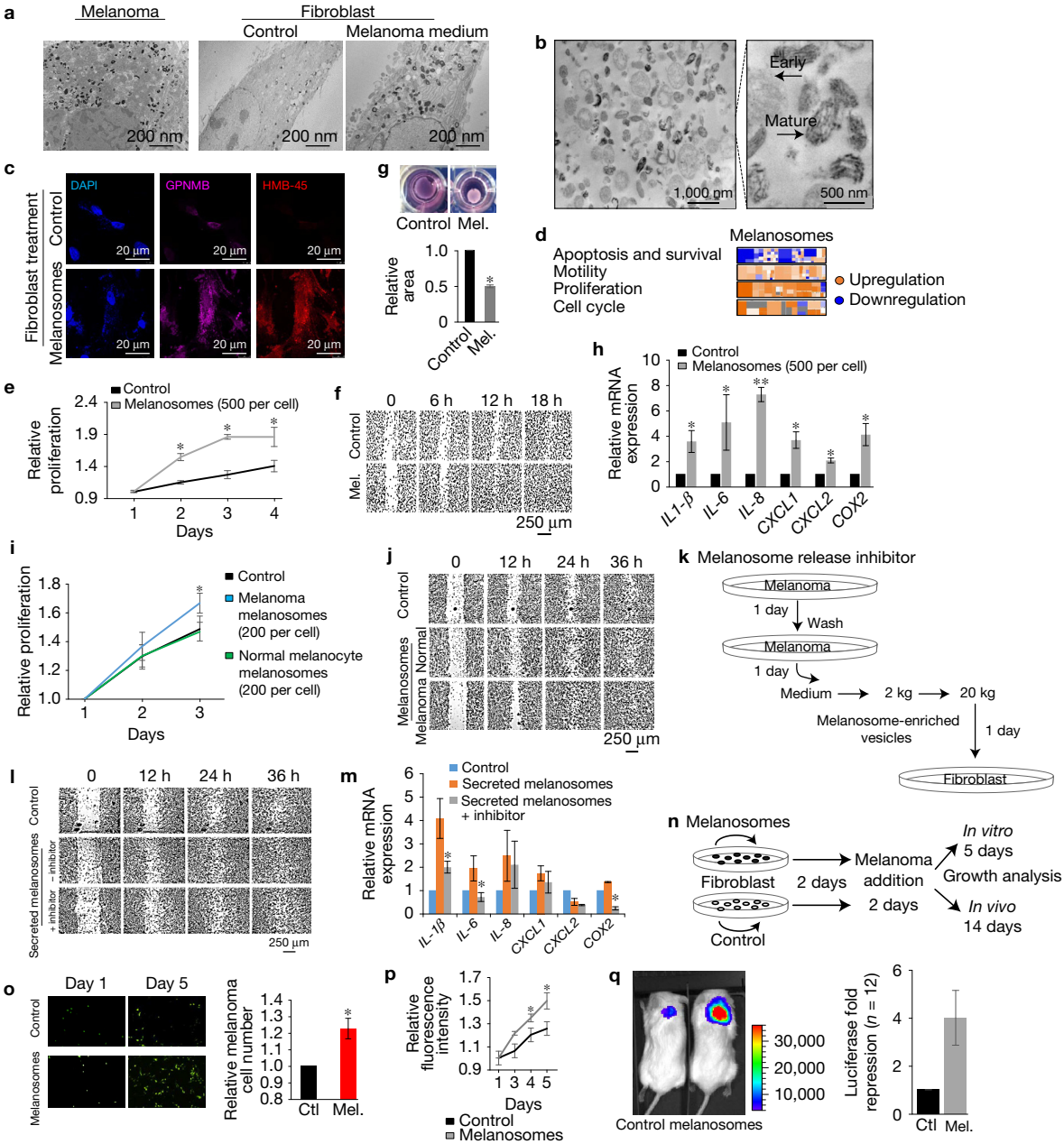

Figure 2 Transfer of melanoma melanosomes into fibroblasts leads to reprogramming. (**a**) Electron microscopy of MNT-1 cells (left), control fibroblasts (middle) and fibroblasts treated with conditional MNT-1 medium (right). (**b**) Electron microscopy of isolated melanosomes (left). An enlargement of one field is shown (right). (**c**) Immunofluorescence staining of the melanosomal markers GPNMB and HMB-45 in melanosome-treated fibroblasts (500 particles per cell). DAPI-stained nuclei are blue. (**d**) Gene profiles of melanoma melanosome-treated and untreated fibroblasts were compared. Heat maps of functional predictions from an IPA analysis are shown. Each rectangle represents one function; the size correlates with the number of involved genes; orange indicates activation, blue attenuation. (**e**) Growth rates of fibroblasts treated with melanoma melanosomes or vehicle (control); $n=3$ independent experiments. (**f**) Migration of fibroblasts treated with melanoma melanosomes (500 particles per cell) or vehicle. Mel., melanosomes. (**g**) Collagen contraction assay of control and melanoma melanosome-treated fibroblasts (500 particles per cell); $n=4$ independent experiments. (**h**) Pro-inflammatory gene signature in fibroblasts following melanoma melanosome treatment. Data were normalized to *GAPDH*; $n=5$ independent experiments. $^{**}P<0.01$. (**i**) Growth rates of fibroblasts treated with 200 particles per cell of melanoma melanosomes, normal melanocyte melanosomes or vehicle; $n=4$ independent experiments. (**j**) Migration of fibroblasts treated with 200 particles per cell of melanoma melanosomes, normal melanocyte melanosomes or vehicle. (**k**) Experimental design scheme. (**l**) Fibroblast migration following treatment as in **k**. Untreated fibroblasts were used as a control. (**m**) Gene levels in fibroblasts following treatment as in **k**. Data were normalized to *GAPDH*; $n=4$ independent experiments. (**n**) Experimental design scheme. (**o**) Left: images of GFP-labelled WM3682 melanoma cells co-cultured with fibroblasts pre-treated with melanosomes or PBS (control). Right: relative number of WM3682 cells (green) from total cells by FACS analysis; $n=3$ independent experiments. Ctl, control. (**p**) Growth rates of WM3268 cells after co-culture with fibroblasts pre-treated with melanosomes or PBS (control); $n=5$ independent experiments. (**q**) WM3526 cells stably transfected with a firefly luciferase reporter were co-cultured with fibroblasts pre-treated with melanosomes or PBS (control) and co-grafted into immunodeficient mice. The graph represents the average bioluminescence activity 14 days post injection; $P=0.054$, $n=12$ mice for each group in 6 independent experiments. In all relevant panels, error bars represent ± s.e.m.; * indicates $P<0.05$. Source data are available in Supplementary Table 8.

clear upregulation in the expression of genes encoding the pro-inflammatory molecules IL1-β, IL-6, IL-8, CXCL1, CXCL2 and COX2 (Fig. 2h). Osteopontin[25], a known CAF inducer, was used as a positive control (Supplementary Fig. 3i). These results suggest that melanoma melanosomes reprogram primary fibroblasts into CAFs.

Treatment of primary fibroblasts with melanosomes from normal human melanocytes or with liposomes (average size 450 nm) resulted in no change in fibroblast proliferation and migration (Fig. 2i,j and Supplementary Fig. 4a–c), but partial upregulation of the pro-inflammatory gene signature was observed after treatment with normal melanosomes. However, this effect was lower than after treatment with melanoma melanosomes (Supplementary Fig. 4d). No effect was observed on pro-inflammatory gene expression after liposome treatment (Supplementary Fig. 4e). On average, about 400 melanosomes or liposomes were taken up per fibroblast (Supplementary Fig. 4f–h). These data suggest that vesicle content rather than size or amount is the key factor regulating cellular effects, strengthening our hypothesis that tumour melanosomes reprogram primary fibroblasts into CAFs.

Melanoma cells also transmit other types of microvesicle, including exosomes, but most vesicles secreted are melanosomes (Supplementary Fig. 4i). Melanoma cells were treated with SB202190, a p38 inhibitor that inhibits melanosome secretion from melanocytes[39] (experimental design Fig. 2k). Secreted melanosomes were observed by electron microscopy (Supplementary Fig. 4j) and fluorescence-activated cell sorting (FACS; Supplementary Fig. 4k) without exosome contamination. Fibroblasts treated with such melanosomes exhibited significantly reduced migration (Fig. 2l) and decreased pro-inflammatory gene expression (Fig. 2m). SB202190 significantly reduced (sixfold) the number of secreted melanosomes without affecting the exosome number (Supplementary Fig. 4l). Also, a decrease in melanin content in melanoma medium and melanin accumulation in fibroblasts was observed (Supplementary Fig. 4m), indicating that SB202190 treatment reduces melanosome release. Additionally, downregulation of tyrosinase expression was observed in fibroblasts (Supplementary Fig. 4n), indicating decreased melanosome absorption. The inhibitor itself did not induce phenotypic changes in melanoma cells (Supplementary Fig. 4o,p) or fibroblasts (Supplementary Fig. 4q,r). These results suggest that inhibition of melanosome transfer from melanoma cells to fibroblasts abrogates fibroblast reprogramming into CAFs.

CAFs are known to enhance proliferation of cancer cells[20]; therefore, we examined whether melanosome-treated fibroblasts promoted melanoma proliferation *in vitro* and *in vivo*. Melanosome-treated or untreated fibroblasts were co-cultured with WM3682 melanoma cells, which stably express GFP (experimental design Fig. 2n). There was a clear induction of melanoma growth *in vitro* when the fibroblasts had been pre-treated with melanosomes (Fig. 2o,p). Similarly, in co-grafted mice, more aggressive melanoma growth was observed when melanoma cells were injected with fibroblasts that had been treated with melanosomes (Fig. 2q). Taken together, our data indicate that melanosomes secreted from melanoma cells promote fibroblast reprogramming into CAFs contributing to cancer progression.

Identification of melanosomal miRNAs

To identify the molecular effectors in melanosomes, we dissected the melanosome content. Published melanosomal protein profiles revealed mainly proteins related to pigmentation and melanosome structure[5]. Interestingly, the protein profile includes proteins with RNA-binding domains. We therefore hypothesized that melanosomes might include RNA. Melanoma exosomes contain functional RNAs, and miRNAs are thought to mediate communication with non-cancerous cells to promote tumour growth[40,41]. However, melanosomal RNAs have not been characterized. Surprisingly, we found that RNA in mature melanosomes from melanoma cells differed in size compared with cellular RNA (Fig. 3a). To confirm that the RNA was inside the melanosomes, an RNase and trypsin treatment of intact melanosomes was performed before RNA isolation. This yielded a clear small RNA population (Fig. 3a), indicating that the small RNA is inside melanosomes and not bound to external structures or macromolecules. It also demonstrated its stability, suggestive of functionality *in vivo*. We subjected melanosomal RNA to size separation. Only molecules of 30–200 nucleotides were found in mature melanosomes pre-treated with RNase; there was no ribosomal RNA as observed in total RNA from MNT-1 cells (Fig. 3b). These assessments showed that isolated melanosomes contain substantial amounts of small RNA.

We next estimated the fraction of melanosomes that contain RNA. For melanosome labelling, MNT-1 cells were transfected with a cDNA construct encoding tyrosinase fused to the fluorescent mCherry. The cells were treated with SYTO RNAselect[42], which labels RNA, grown in fresh medium and subjected to FACS analysis. About 90% of tyrosinase-expressing melanosomes contained RNA (Fig. 3c). To further analyse the small RNA population, miRNA profiling was performed for MNT-1 cells, pre-mature melanosomes, mature melanosomes, secreted melanosomes and exosomes (Fig. 3d and Supplementary Fig. 5a and Supplementary Table 5). Since mature melanosomes move to neighbouring cells, the 100 most highly expressed miRNAs from mature melanosomes were compared with expression levels in pre-mature melanosomes (Supplementary Table 3). Only five miRNAs previously associated with melanoma[43,44] were expressed at higher levels in mature melanosomes: miR-149, miR-211, miR-23, miR-let7a and miR-let7b (Fig. 3d). This miRNA expression signature was validated by quantitative real-time PCR (qRT-PCR) (Supplementary Fig. 5b).

Melanosomal miRNA trafficking into fibroblasts

We examined the melanosomes' ability to transfer RNA into fibroblasts. Melanosomes of MNT-1 cells were double labelled with fluorescent tyrosinase (mCherry) and an RNA-specific fluorophore as in Fig. 3c. Melanoma medium was added to fibroblasts. Co-localization of tyrosinase and labelled RNA in the fibroblasts indicated RNA transfer through melanosomes (Fig. 4a). In addition, FACS analyses demonstrated that all tyrosinase-expressing melanosomes taken up by fibroblasts contained RNA (Fig. 4b).

To examine which miRNAs were transferred, the five melanoma-related miRNAs (Fig. 3d; miR-149, miR-211, miR-23, miR-let7a, miR-let7b) were quantified by qRT-PCR in fibroblasts before and after melanosome treatment. The miR-211 level increased most significantly (Supplementary Fig. 5c). We therefore focused on the effect of miR-211. As a control, we used miR-320c, which was the most enriched in melanosomes compared with whole cells (Supplementary Fig. 5d). To exclude the possibility that mature miR-211 or miR-320

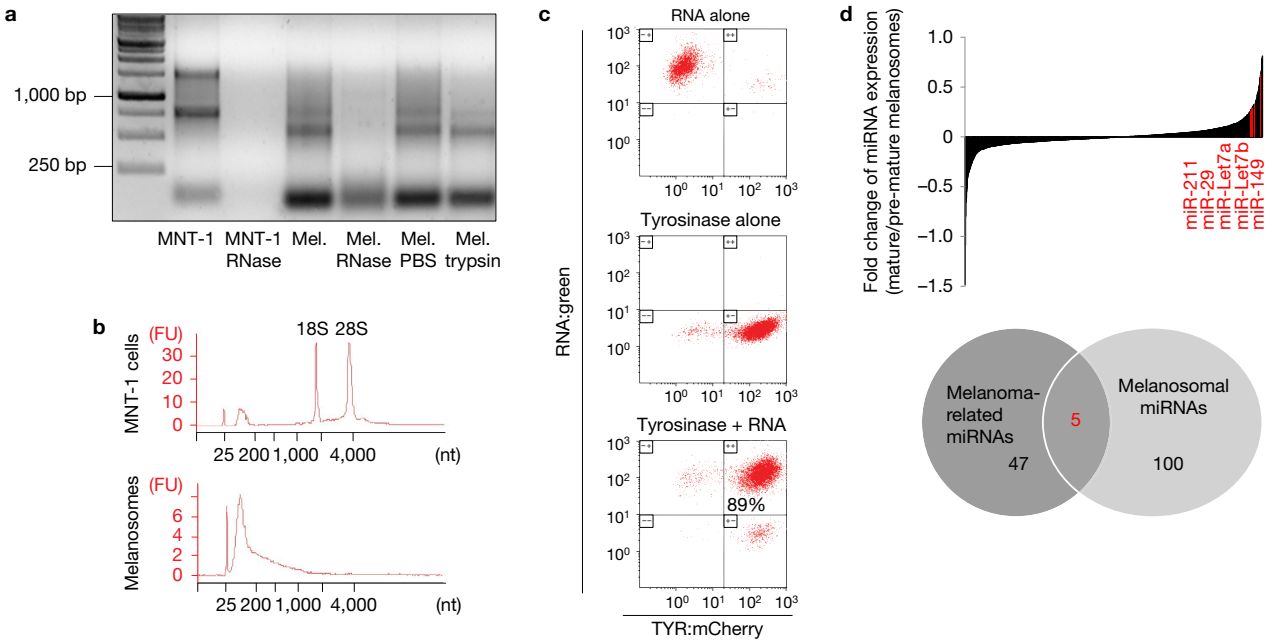

Figure 3 Identification of melanosomal miRNAs. (**a**) Electrophoretic separation of total RNA isolated from whole MNT-1 cells or mature melanosomes (Mel.) treated with RNase, trypsin or PBS as a control. DNA marker was used. (**b**) RNA analysis in microchannels of a bioanalyser of total RNA isolated from MNT-1 cells (upper panel) or mature melanosomes after treatment with RNase (lower panel). FU, fluorescence units; nt, nucleotides. (**c**) FACS analysis of melanoma melanosomes labelled with tyrosinase–mCherry fusion and with SYTO RNAselect (green). Melanosomes with RNA labelling (RNA alone), melanosomes expressing tyrosinase–mCherry (tyrosinase alone), and melanosomes with RNA and melanosome labelling (tyrosinase and RNA) were analysed. Of total melanosomes, 89% were double labelled. (**d**) Fold differences in miRNA expression in mature and pre-mature melanosomes (upper panel). A Venn diagram shows the overlap between miRNAs enriched in mature melanosomes and previously identified melanoma-related miRNAs[43,44] (lower panel). The five common molecules are highlighted in red in the upper panel.

was produced in the fibroblasts, pre-miR-211 and pre-miR-320c levels were examined. There were significant increases in mature miRNA levels in fibroblasts following melanosome treatment, but no changes in pre-miR levels (Fig. 4c,d). To further validate the transfer of mature miRNAs through melanosomes, melanosomes were extracted from human MNT-1 cells and added to NIH/3T3 cells (mouse fibroblasts). No change was observed in mouse miR-211 levels, whereas both human miR-211 and human miR-320c were detected (Fig. 4e,f). In addition, mouse miR-211 was found in human fibroblasts after treatment with melanosomes isolated from mouse B16F10 melanoma cells (Supplementary Fig. 5e,f), verifying the transfer of miRNAs via melanosomes.

Interestingly, normal melanosomes contain less miR-211 than melanoma melanosomes (Supplementary Fig. 5g). An elevation in miR-211 was observed as melanosomes matured from pre- to mature to secreted melanoma melanosomes (Supplementary Fig. 5h). Moreover, a decrease in secreted miR-211 was observed after treatment of melanoma cells with the melanosome release inhibitor SB202190 (Supplementary Fig. 5i). This evidence backs our hypothesis that there is a specific transport of miR-211 into adjacent fibroblasts to promote cancer development.

Fibroblast reprogramming into CAFs is melanosomal miR-211 dependent

Next, we determined whether miR-211 and miR-320c contribute to the reprogramming of fibroblasts. Cells were treated with miR-211 or miR-320c and the mRNA profile was compared to that from fibroblasts treated with scrambled miR. Again, a functional gene set enrichment analysis was performed on the basis of the 10% most differentially expressed genes (Supplementary Table 2). Similar to melanosome treatment, miR-211 treatment resulted in expression changes associated with proliferation and cell motility (Fig. 5a). With miR-320c, no such variation was observed. In addition, miR-211 increased cell growth and migration compared with miR-320c or scrambled miR (Fig. 5b,c and Supplementary Fig. 6a,b). Also, miR-211, but not miR-320c, led to a significant increase in collagen contraction (Fig. 5d and Supplementary Fig. 6c) and elevated expression of the pro-inflammatory genes *IL1*-β, *IL-6*, *IL-8*, *CXCL1* and *CXCL2* (Fig. 5e and Supplementary Fig. 6d). These results indicate that melanosomal miR-211 reprograms primary fibroblasts into CAFs and suggest that downregulation of miR-211 inhibits CAF formation. Indeed, antagomir-mediated depletion of miR-211 in primary fibroblasts before melanosome treatment significantly decreased the effect of melanosome treatment on fibroblast migration and pro-inflammatory gene expression (Fig. 5f,g).

Finally, we examined miR-211 expression in clinical sections using *in situ* hybridization. In normal skin, miR-211 appeared in the epidermis, as expected[2]. In melanoma, we observed miR-211 in the tumour stroma (Fig. 5h and Supplementary Fig. 6e). We validated our findings in a transplantable melanoma mouse model utilizing the Ret melanoma-derived cell line[45]. Ret cells are capable of transferring miR-211 into fibroblasts (Supplementary Fig. 6f). Next, melanoma-associated fibroblasts were isolated by FACS from fresh tumour tissues and analysed for miR-211; we observed a significant

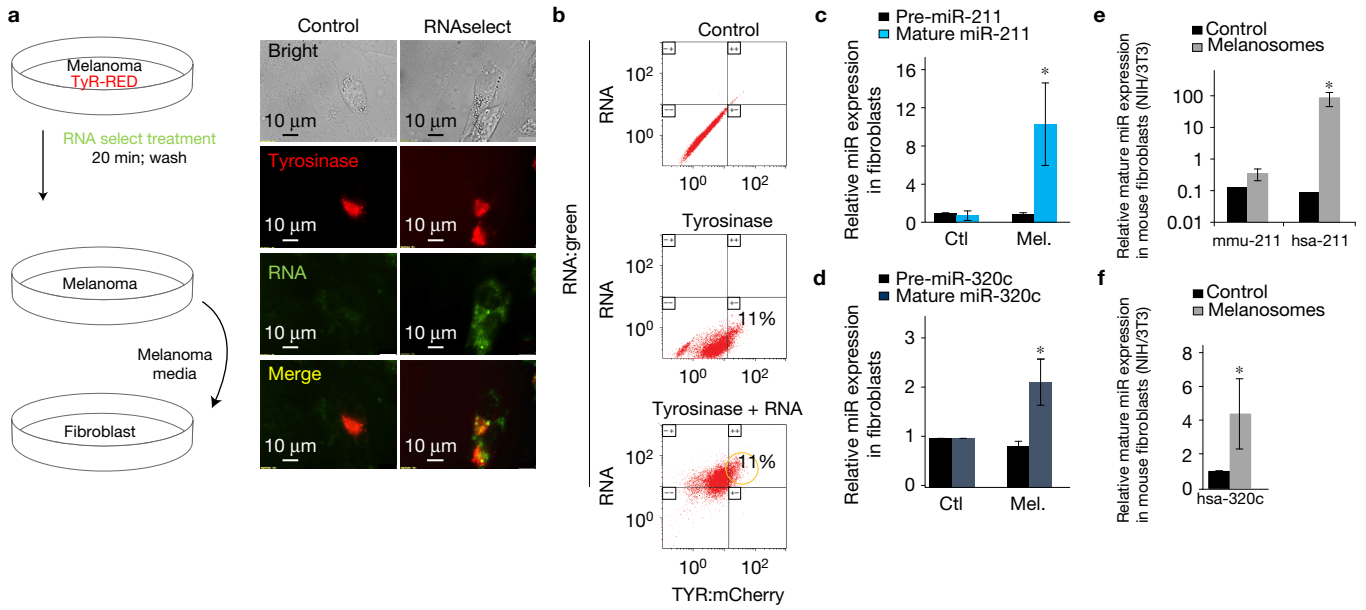

Figure 4 Melanosomal miRNA trafficking into fibroblasts. (**a**) Left panel: experimental design scheme. Right panel: imaging of fluorescence staining (green) of fibroblasts treated with melanoma medium that contained melanosomes in which there was labelled (SYTO RNAselect) or unlabelled RNA (control). Melanosomes expressing labelled tyrosinase appear in red. (**b**) FACS analysis of fibroblasts treated with melanoma medium containing melanosomes labelled with tyrosinase–mCherry fusion (tyrosinase) and fibroblasts treated with melanoma medium containing melanosomes labelled with tyrosinase–mCherry fusion and SYTO RNAselect-labelled RNA (tyrosinase and RNA). As a control, fibroblasts were treated with melanoma medium (control). Double-labelled melanosomes are indicated by yellow circles. (**c**) Levels of mature and pre-miRNA of miR-211 in fibroblasts treated with melanosomes (Mel.) or PBS (Ctl). Data were normalized to *RNU6B* and *GAPDH* levels, respectively. Error bars represent ± s.e.m., * indicates $P<0.05$ ($n=3$ independent experiments). (**d**) Levels of mature and pre-miRNA of miR-320c in fibroblasts treated with melanosomes (Mel.) or PBS (Ctl). Data were normalized to *RNU6B* and *GAPDH* levels. Error bars represent ± s.e.m., * indicates $P<0.05$ ($n=5$ independent experiments). (**e**) Mature mouse mmu-miR-211 and human hsa-miR-211 levels were determined in mouse fibroblasts (NIH/3T3) that were treated with melanosomes isolated from human melanoma cells or with PBS. Data were normalized to *RNU6B* levels. Error bars represent ± s.e.m., * indicates $P<0.05$ ($n=6$ independent experiments). (**f**) Mature human miR-320c levels (hsa-miR-320c) were measured in mouse fibroblasts (NIH/3T3) that were treated with melanosomes isolated from human melanoma cells or with PBS. Data were normalized to *RNU6B* levels. Error bars represent ± s.e.m., * indicates $P<0.05$ ($n=3$ independent experiments). Source data are available in Supplementary Table 8.

increase in miR-211 expression compared with normal mouse fibroblasts (Fig. 5i). To validate the purity of the sorted cell population, known markers of melanoma, fibroblasts and immune cells were analysed (Supplementary Fig. 6g). Melanoma-associated fibroblasts did not contain tyrosinase mRNA but the tyrosinase protein, indicating that tyrosinase protein was imported through uptake of melanosomes (Supplementary Fig. 6g,h). These results strongly imply that the transfer of melanosomal miR-211 to fibroblasts contributes to CAF reprogramming in the melanoma microenvironment.

Melanosomal miR-211 induces CAF formation via upregulation of MAPK signalling

For identification of the targets of melanosomal miR-211 in fibroblasts, the 2,000 most downregulated genes following miR-211 expression were overlapped with the 2,000 most downregulated genes following melanosome treatment, predicted target genes of miR-211 and known CAF-related genes (Fig. 6a and Supplementary Fig. 7a and Supplementary Table 4). Comparison revealed four common genes: *ANGPT2*, *IGF2R*, *SHC1* and *PDGFRB*. Among them, the mRNA encoding insulin-like growth factor 2 receptor (IGF2R) is the only validated target of miR-211[12]; IGF2R is a tumour suppressor in several cancers[46,47]. *IGF2R* mRNA levels decreased in fibroblasts that were treated with miR-211 or melanosomes (Fig. 6b). Next, primary fibroblasts were transfected with a luciferase reporter gene containing the *IGF2R* 3′-UTR with the wild-type or a mutated miR-211-binding site. Overexpression of miR-211 or melanosome treatment caused a decrease in the wild-type reporter signal, whereas cells containing the mutated binding site exhibited no such repression (Fig. 6c). These results indicate that *IGF2R* is a direct target of melanosomal miR-211 in fibroblasts.

One function of IGF2R is to bind to the ligand IGF2, leading to IGF2 degradation and consequently an inhibition of the growth stimulation that results from the interaction between IGF2 and IGF1R[48,49]. IGF2 is upregulated in CAFs[50], suggesting that IGF2R is inhibited. Therefore, reduction in IGF2R following treatment with miR-211 or melanosomes may increase IGF2 levels, promoting its binding to IGF1R, and thus leading to hyperactivation of this pathway and increased proliferation. To analyse the signalling downstream of IGF1R, a network and a canonical pathway were generated using the IPA software. The network includes genes downstream of IGF1R that are known to be associated with fibroblast proliferation and migration. Connecting the network and the canonical pathway to the mRNA profiling data of fibroblasts treated with miR-211 or melanosomes revealed in both cases an upregulation of ERK (Fig. 6d and Supplementary Fig. 7b). The analysis indicated that MAPK signalling could be responsible for the fibroblast reprogramming.

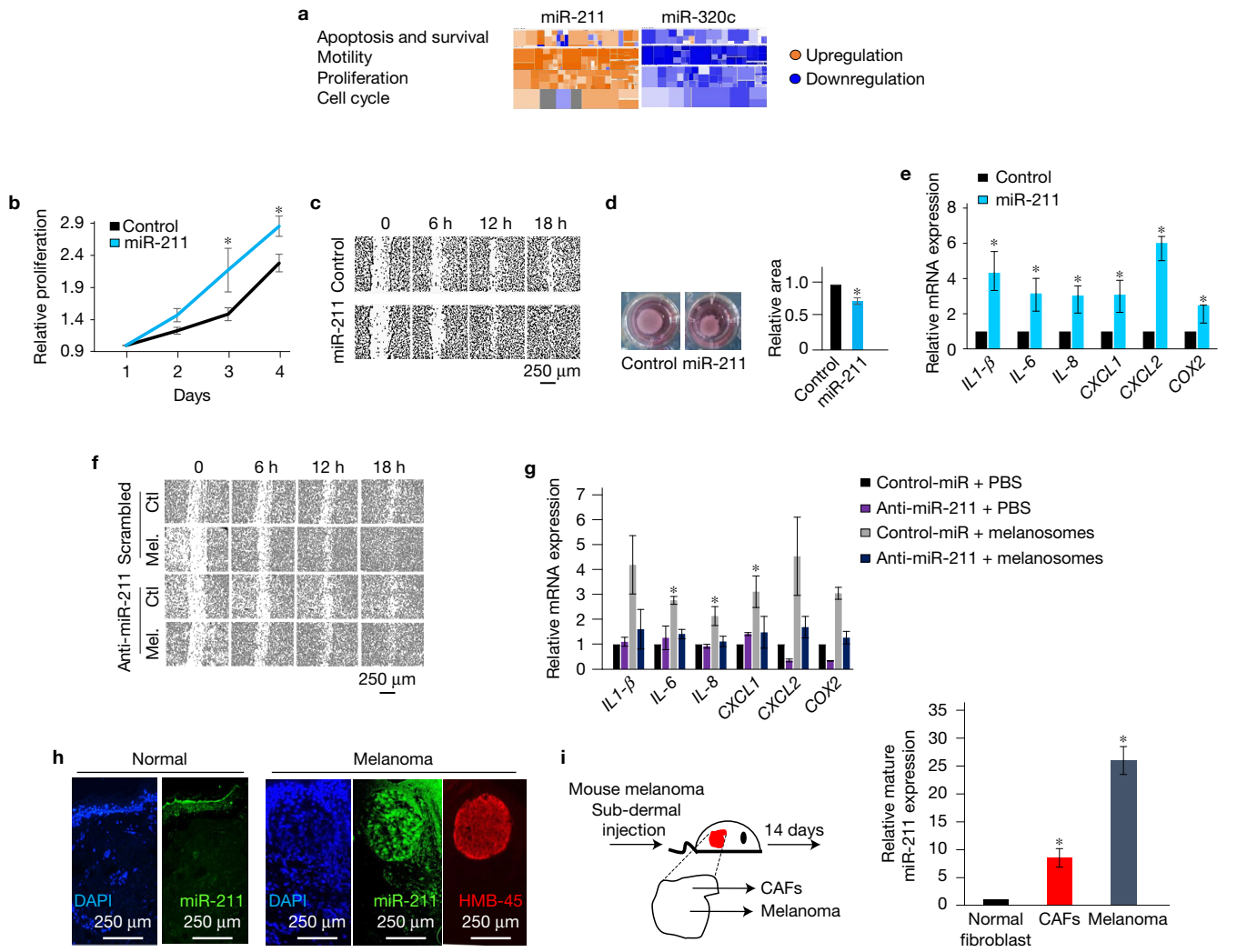

Figure 5 Fibroblast reprogramming into CAFs is melanosomal miR-211 dependent. (**a**) Fibroblasts transfected with miR-211 or miR-320c were compared with fibroblasts transfected with a scrambled miR mimic (as control). Heat maps of functional predictions resulting from an IPA analysis of mRNA profiles are shown. Each rectangle represents one function; the size correlates with the number of involved genes; colour gradations indicate the predicted activation state (orange indicates activation, blue indicates attenuation). (**b**–**e**) Fibroblasts transfected with miR-211 or scrambled miR (control) were analysed. (**b**) Growth rates were determined. Error bars represent ± s.e.m., * indicates $P < 0.05$ ($n = 5$ independent experiments). (**c**) Cell migration was tested by a scratch assay. (**d**) Collagen remodelling capacity was examined by a three-dimensional collagen contraction assay. Error bars represent ± s.e.m., * indicates $P < 0.05$ ($n = 3$ independent experiments). (**e**) The pro-inflammatory gene signature was evaluated by qRT-PCR. Data were normalized to *GAPDH* levels. Error bars represent ± s.e.m., * indicates $P < 0.05$ ($n = 3$ independent experiments). (**f**,**g**) Fibroblasts were transfected with an anti-miR-211 or scrambled miR and then treated with melanosomes (Mel.) or PBS (Ctl). (**f**) Migration was analysed in a scratch assay. (**g**) Pro-inflammatory gene expression was analysed; data were normalized to *GAPDH* levels. Error bars represent ± s.e.m., * indicates $P < 0.05$ ($n = 3$ independent experiments). (**h**) miR-211 expression levels in normal human skin and melanoma specimen detected by *in situ* hybridization (green). HMB-45-stained melanoma cells (red) and DAPI-stained nuclei (blue). (**i**) Levels of mature miR-211 in normal fibroblasts (normal fibroblast), melanoma-associated fibroblasts (CAFs) and melanoma cells. Data were normalized to *RNU6B*. Error bars represent ± s.e.m., * indicates $P < 0.05$ ($n = 12$ mice for treatment and 4 for control in 4 independent experiments). Source data are available in Supplementary Table 8.

Following miR-211 transfection or melanosome treatment of fibroblasts, we observed an elevation in the phospho-ERK levels, a marker for MAPK signalling activation, and an increase in phospho-IGF1R; no change occurred in the total ERK or IGF1R levels (Fig. 6e). This suggests that the activation of MAPK signalling is mediated by IGF1R. To verify this, we inhibited MAPK signalling using the ERK inhibitor U0126 concurrently with miR-211 transfection or melanosome treatment (Fig. 6f). In the presence of U0126, the effect of miR-211 and melanosomes on fibroblast migration, proliferation and on the expression of pro-inflammatory markers was abolished (Fig. 6g–i).

Finally, we analysed the relevance of miR-211 in melanoma progression by examining IGF2R expression in the stroma adjacent to primary human and mouse melanoma. Melanoma-associated fibroblasts were isolated by FACS from fresh mouse tumour tissues (as in Fig. 5i). A decrease in *IGF2R* mRNA expression was observed in melanoma-associated fibroblasts compared with normal fibroblasts (Fig. 7a). Moreover, a decrease in IGF2R and an increase in

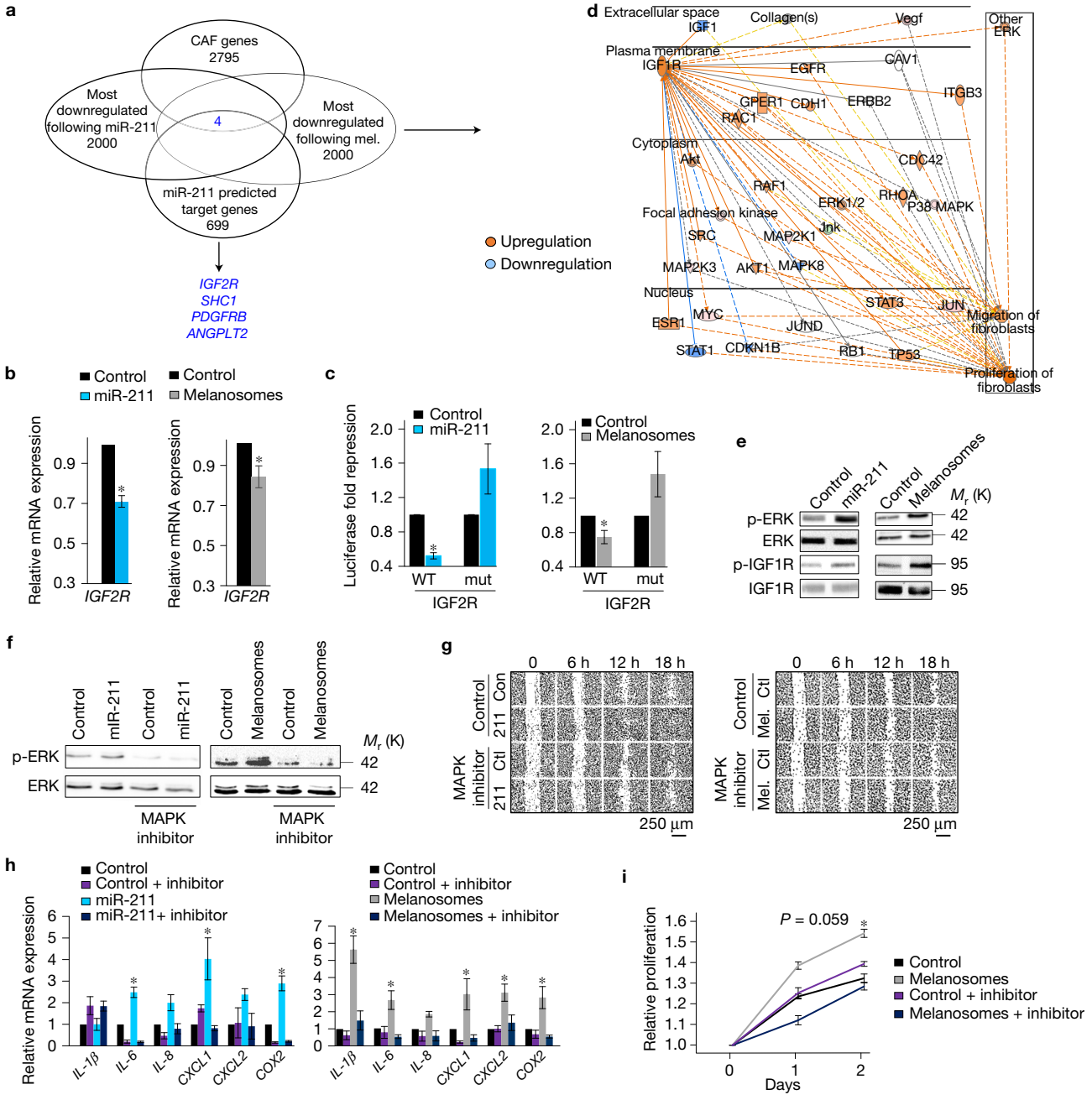

Figure 6 Melanosomal miR-211 induces CAF formation via upregulation of MAPK signalling. (**a**) Overlap between the 2,000 most downregulated genes in fibroblasts following miR-211 or melanosome treatment, predicted miR-211 targets (http://www.targetscan.org) and CAF-related genes (genecards.org). (**b**) *IGF2R* mRNA levels in fibroblasts after treatment with miR-211 ($n=3$ independent experiments) or melanosomes ($n=5$ independent experiments). Data were normalized to *GAPDH* levels. (**c**) NIH/3T3 cells with luciferase constructs containing the wild-type or mutated miR-211-binding site in the 3′-UTR of *IGF2R* were treated with miR-211 or melanosomes. Scrambled miR sequences or PBS served as controls. Firefly luciferase activity was measured and normalized to *Renilla* luciferase activity; $n=5$ independent experiments. (**d**) IPA network for IGF1R signalling; all genes downstream of IGF1R and related to fibroblast proliferation and migration were coloured according to their expression level in miR-211-transfected fibroblasts compared with control fibroblasts (scrambled). Up- and downregulated genes are labelled red or green, respectively; predicted activation is shown in orange, inhibition in blue. The dashed lines represent indirect relationships, and the solid lines represent direct relationships. Orange arrows: activation; blue arrows: inhibition; yellow arrows: inconsistency between observation and prediction; grey arrows: lack of supporting data. (**e**) Phospho- and total ERK and IGF1R levels in fibroblasts treated with miR-211 or melanosomes. Scrambled miR or PBS treatments were used as controls. (**f**) Phospho- and total ERK in fibroblasts treated with miR-211 or melanosomes in the presence or absence of the MAPK inhibitor U0126. Scrambled miR or PBS treatments were used as controls. (**g**) Fibroblast migration following miR-211 or melanosome treatment and addition of the MAPK inhibitor U0126. (**h**) Pro-inflammatory gene signatures in fibroblasts treated as in **g**, normalized to *GAPDH*; $n=3$ independent experiments. (**i**) Growth rates of fibroblasts treated with melanosomes in the presence or absence of MAPK inhibitor ($n=5$ samples, 3 independent experiments). In all relevant panels, error bars represent ± s.e.m.; * indicates $P<0.05$. Unprocessed original scans of blots are shown in Supplementary Fig. 8. Source data are available in Supplementary Table 8.

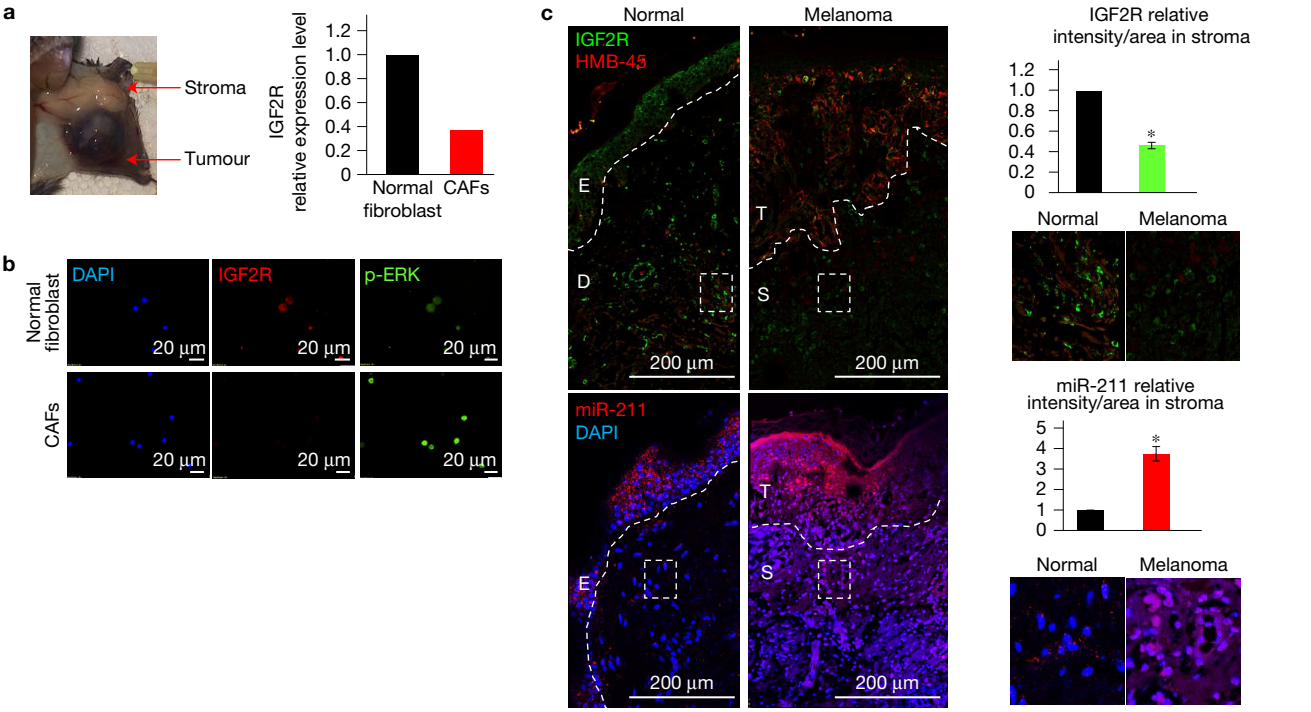

Figure 7 Melanosomal miR-211 induces CAF formation via upregulation of MAPK signalling *in vivo*. (**a**) Left: representative image of melanoma and adjacent stroma in a melanoma mouse model. Right: levels of IGF2R in normal fibroblasts and CAFs, normalized to GAPDH ($n=20$ mice from two independent experiment). (**b**) Immunostaining of IGF2R and phospho-ERK in isolated CAFs or normal fibroblasts. DAPI-stained nuclei are blue. (**c**) Immunofluorescence staining of HMB-45 and IGF2R (top), *in situ* hybridization of miR-211 and DAPI-stained nuclei (bottom) in normal human skin and human melanoma sections. Dashed lines separate epidermis (E) and dermis (D); tumour (T) and stroma (S) are labelled. Magnifications (×63) of areas marked by squares appear on the right. Graphs represent the quantification of IGF2R and miR-211 fluorescence intensities; $n=50$ cells from 5 human pathological sections. Error bars represent ± s.e.m.; * indicates $P<0.05$. Source data are available in Supplementary Table 8.

phospho-ERK were observed in fibroblasts isolated from melanoma stroma (Fig. 7b). We then evaluated the correlation between IGF2R and miR-211 expression in a cohort of melanoma patient tumours using immunohistochemistry and *in situ* hybridization, respectively. A 60% decrease in IGF2R levels and a fourfold increase in miR-211 levels were observed in melanoma dermal fibroblasts compared with normal fibroblasts (Fig. 7c and Supplementary Fig. 7c–f). Finally, to support the hypothesis that melanoma-secreted vesicles vary as cancer progresses, we have performed miRNA profiling of a melanoma cell line with high invasion ability[51]. We compared the data with that from MNT-1 cells, which represent melanoma at early stage with no invasion abilities. Our analysis revealed that as melanoma progresses and gains invasion abilities, the miRNA content changes to a miRNA signature that reflects the invasion potential[52] (Supplementary Fig. 7g–j and Supplementary Table 6). Taken together, our data show that miR-211, contained in melanosomes that are secreted by melanoma cells and taken up by fibroblasts, activates MAPK signalling and triggers fibroblast reprogramming into CAFs (Supplementary Fig. 7k).

DISCUSSION

Starting from clinical evidence, we uncovered a communication route between melanoma cells and the microenvironment that contributes to the generation of the tumour primary niche (illustrated in Supplementary Fig. 7k) by fibroblast accumulation in the dermis before melanoma invasion. Although α-SMA expression is a major characteristic of CAFs[26], we did not observe an expression increase following melanosome treatment or miR-211 expression. This agrees with reports that α-SMA is not necessary for CAF formation and activation[23,33]. The effects of miR-211 expression in fibroblasts on proliferation and contraction were not as large as those of melanosome treatment, indicating that additional factors in melanosomes are involved in CAF formation.

Like normal melanocytes, melanoma cells have the ability to produce and transfer melanosomes to neighbouring cells[7,8]. However, melanoma melanosomes and normal melanosomes contain a different spectrum of miRNAs. Consistently, fourfold less miR-211 was observed in the dermis of normal skin compared with amounts in *in situ* melanoma. This difference suggests that these vesicles are likely to promote different phenotypic changes in receiver cells. In addition to melanosomes, melanoma cells transmit other types of microvesicle, including exosomes. Exosomes contain functional mRNAs, miRNAs and proteins that can alter the cellular environment to favour tumour growth[40,41,53], and tumour exosomes contribute to fibroblast activation[54]. Although our data do not exclude the possibility that melanoma exosomes play a role in CAF formation, it is crucial to discuss the timing in the tumour development stage at which these vesicles act. We studied the role of microvesicles at the very early stages of melanoma development, when melanoma cells have yet to invade the dermis. Exosomes have a role in long-distance metastases, the late

stages of melanoma progression[40]. As melanoma progresses, there is a dramatic change in the secreted vesicle population and content[40]. At stage IV, an increase in exosome number and an elevation in expression of tyrosinase and MART1 are observed in these exosomes, relative to primary tumours[40,55]. Moreover, melanoma pigmentation demonstrates a plasticity phenotype: it is high in primary tumours, low in invasive cells, and high again in metastases[56]. This suggests that the production of melanosomes, like the production of exosomes, depends on disease stage.

We did not detect tyrosinase, DCT or GPNMB in MNT-1 exosomes, and no exosome markers in isolated melanosomes. This is in agreement with our clinical observation that melanosomes, and not exosomes, were detected in the dermal fibroblasts. Moreover, we have performed miRNA profiling of secreted melanosomes and exosomes. About 70% of miRNAs are shared; however, exosomes have unique miRNAs that are enriched for those with functions in WNT signalling, whereas melanosomes are enriched in miRNAs involved in ERB signalling and its downstream MAPK signalling, as determined by KEGG analysis. This strengthens our hypothesis that melanoma melanosomes induce CAF formation by the activation of MAPK signalling in fibroblasts. It is possible that melanosomes can be transferred also to other cells in the melanoma microenvironment, such as immune or endothelial cells, and have additional effects on cancer progression. □

METHODS

Methods, including statements of data availability and any associated accession codes and references, are available in the online version of this paper.

Note: Supplementary Information is available in the online version of the paper

ACKNOWLEDGEMENTS

This work was supported in part by the Cooperation Program in Cancer Research of the Deutsches Krebsforschungszentrum (DKFZ) and Israel's Ministry of Science, Technology and Space (MOST) and by the Israel Science Foundation (ISF). We thank the microarray unit of the DKFZ Genomics and Proteomics Core Facility for performing microarray analyses on the Illumina Human Sentrix-12 BeadChip array and the Agilent Human miRNA Microarray.

AUTHOR CONTRIBUTIONS

S.D. designed the experimental approach, performed experimental work, analysed data and wrote the manuscript. L.S. conducted experimental work, miRNA and gene expression studies, exosomes analysis, and analysis of the microarray data. H.S. and N.E. conducted *in vivo* experiments, and FACS sorting, and added discussion on CAFs formation, D.S., Y.D. and H.M. conducted melanosome isolation and RNA detection experiments. A.Zilberberg conducted immunofluorescence staining and tyrosinase activity assays. L.L. helped in establishing the melanosome isolation protocol. S.G., A.B., I.B., R.B., P.G. and H.V. provided human skin and melanoma specimens and edited the manuscript. A.Zinger and A.S. generated the labelled liposomes and performed their analysis. T.G. performed the liposome uptake analysis. O.B. provided critical discussion and aided in writing of the manuscript. Y.F. and M.N. performed the electronic microscopy analysis. V.I. provided normal human melanocytes. J.D.H. coordinated the project, analysed and provided gene expression study data, and participated in writing of the manuscript. C.L. developed the hypothesis, designed the experimental approach, coordinated the project, and wrote the manuscript. S.A. conducted the exosome experiment analysis. M.K. designed and cloned the tyrosinase:mCherry plasmid.

COMPETING FINANCIAL INTERESTS

The authors declare no competing financial interests.

Published online at http://dx.doi.org/10.1038/ncb3399
Reprints and permissions information is available online at www.nature.com/reprints

1. Bell, R. E. & Levy, C. The three M's: melanoma, microphthalmia-associated transcription factor and microRNA. *Pigment Cell Melanoma Res.* **24,** 1088–1106 (2011).
2. Raposo, G. & Marks, M. S. Melanosomes - dark organelles enlighten endosomal membrane transport. *Nat. Rev. Mol. Cell Biol.* **8,** 786–797 (2007).
3. Watabe, H., Kushimoto, T., Valencia, J. C. & Hearing, V. J. in *Current Protocols in Cell Biology* (eds Bonifacino, J. S. *et al.*) Ch. 3, Unit 3, 14 (2005).
4. Joshi, P. G. Melanocyte–keratinocyte interaction induces calcium signalling and melanin transfer to keratinocytes. *Pigment Cell Res.* **20,** 380–384 (2007).
5. Yamaguchi, Y. & Hearing, V. J. Physiological factors that regulate skin pigmentation. *Biofactors* **35,** 193–199 (2009).
6. Basrur, V. *et al.* Proteomic analysis of early melanosomes: identification of novel melanosomal proteins. *J. Proteome Res.* **2,** 69–79 (2003).
7. Boissy, R. E. Melanosome transfer to and translocation in the keratinocyte. *Exp. Dermatol.* **12,** 5–12 (2003).
8. Lazova, R. & Pawelek, J. M. Why do melanomas get so dark? *Exp. Dermatol.* **18,** 934–938 (2009).
9. Chen, K. G. *et al.* Melanosomal sequestration of cytotoxic drugs contributes to the intractability of malignant melanomas. *Proc. Natl Acad. Sci. USA* **103,** 9903–9907 (2006).
10. Bartel, D. P. MicroRNAs: genomics, biogenesis, mechanism, and function. *Cell* **116,** 281–297 (2004).
11. Lu, J. *et al.* MicroRNA expression profiles classify human cancers. *Nature* **435,** 834–838 (2005).
12. Levy, C. *et al.* Intronic miR-211 assumes the tumor suppressive function of its host gene in melanoma. *Mol. Cell* **40,** 841–849 (2010).
13. Asangani, I. *et al.* MicroRNA-21 (miR-21) post-transcriptionally downregulates tumor suppressor Pdcd4 and stimulates invasion, intravasation and metastasis in colorectal cancer. *Oncogene* **27,** 2128–2136 (2008).
14. Levy, C. *et al.* Lineage-specific transcriptional regulation of DICER by MITF in melanocytes. *Cell* **141,** 994–1005 (2010).
15. Bedrosian, I. *et al.* Incidence of sentinel node metastasis in patients with thin primary melanoma (< or =1 mm) with vertical growth phase. *Ann. Surg. Oncol.* **7,** 262–267 (2000).
16. Sorrell, J. M. & Caplan, A. I. Fibroblast heterogeneity: more than skin deep. *J. Cell Sci.* **117,** 667–675 (2004).
17. Bhowmick, N. A., Neilson, E. G. & Moses, H. L. Stromal fibroblasts in cancer initiation and progression. *Nature* **432,** 332–337 (2004).
18. Kalluri, R. & Zeisberg, M. Fibroblasts in cancer. *Nat. Rev. Cancer* **6,** 392–401 (2006).
19. Servais, C. & Erez, N. From sentinel cells to inflammatory culprits: cancer-associated fibroblasts in tumour-related inflammation. *J. Pathol.* **229,** 198–207 (2013).
20. Orimo, A. *et al.* Stromal fibroblasts present in invasive human breast carcinomas promote tumor growth and angiogenesis through elevated SDF-1/CXCL12 secretion. *Cell* **121,** 335–348 (2005).
21. Tlsty, T. D. & Hein, P. W. Know thy neighbor: stromal cells can contribute oncogenic signals. *Curr. Opin. Genet. Dev.* **11,** 54–59 (2001).
22. Cornil, I. *et al.* Fibroblast cell interactions with human melanoma cells affect tumor cell growth as a function of tumor progression. *Proc. Natl Acad. Sci. USA* **88,** 6028–6032 (1991).
23. Erez, N., Truitt, M., Olson, P., Arron, S. T. & Hanahan, D. Cancer-associated fibroblasts are activated in incipient neoplasia to orchestrate tumor-promoting inflammation in an NF-κB-dependent manner. *Cancer Cell* **17,** 135–147 (2010).
24. Quante, M. *et al.* Bone marrow-derived myofibroblasts contribute to the mesenchymal stem cell niche and promote tumor growth. *Cancer Cell* **19,** 257–272 (2011).
25. Sharon, Y. *et al.* Tumor-derived osteopontin reprograms normal mammary fibroblasts to promote inflammation and tumor growth in breast cancer. *Cancer Res.* **75,** 963–973 (2015).
26. Serini, G. & Gabbiani, G. Mechanisms of myofibroblast activity and phenotypic modulation. *Exp. Cell Res.* **250,** 273–283 (1999).
27. Flach, E. H., Rebecca, V. W., Herlyn, M., Smalley, K. S. & Anderson, A. R. Fibroblasts contribute to melanoma tumor growth and drug resistance. *Mol. Pharm.* **8,** 2039–2049 (2011).
28. Gallagher, P. G. *et al.* Gene expression profiling reveals cross-talk between melanoma and fibroblasts: implications for host-tumor interactions in metastasis. *Cancer Res.* **65,** 4134–4146 (2005).
29. Öhlund, D., Elyada, E. & Tuveson, D. Fibroblast heterogeneity in the cancer wound. *J. Exp. Med.* **211,** 1503–1523 (2014).
30. Mitra, A. K. *et al.* MicroRNAs reprogram normal fibroblasts into cancer-associated fibroblasts in ovarian cancer. *Cancer Discov.* **2,** 1100–1108 (2012).
31. Ruiter, D., Bogenrieder, T., Elder, D. & Herlyn, M. Melanoma–stroma interactions: structural and functional aspects. *Lancet Oncol.* **3,** 35–43 (2002).
32. Haass, N. K., Smalley, K. S., Li, L. & Herlyn, M. Adhesion, migration and communication in melanocytes and melanoma. *Pigment Cell Res.* **18,** 150–159 (2005).
33. Sugimoto, H., Mundel, T. M., Kieran, M. W. & Kalluri, R. Identification of fibroblast heterogeneity in the tumor microenvironment. *Cancer Biol. Ther.* **5,** 1640–1646 (2006).
34. Hoashi, T. *et al.* Glycoprotein nonmetastatic melanoma protein b, a melanocytic cell marker, is a melanosome-specific and proteolytically released protein. *FASEB J.* **24,** 1616–1629 (2010).
35. Torisu, H. *et al.* Macrophage infiltration correlates with tumor stage and angiogenesis in human malignant melanoma: possible involvement of TNFα and IL-1α. *Int. J. Cancer* **85,** 182–188 (2000).

36. Mathivanan, S. & Simpson, R. J. ExoCarta: a compendium of exosomal proteins and RNA. *Proteomics* **9,** 4997–5000 (2009).
37. Sato, I., Miyado, M. & Sunohara, M. NADH dehydrogenase activity and expression of mRNA of complex I (ND1, 51kDa, and 75kDa) in heart mitochondria of klotho mouse. *Okajimas Folia Anat. Jpn.* **82,** 49–56 (2005).
38. Barker, H. E., Bird, D., Lang, G. & Erler, J. T. Tumor-secreted LOXL2 activates fibroblasts through FAK signaling. *Mol. Cancer Res.* **11,** 1425–1436 (2013).
39. Bellei, B., Pitisci, A., Migliano, E., Cardinali, G. & Picardo, M. Pyridinyl imidazole compounds interfere with melanosomes sorting through the inhibition of cyclin G-associated Kinase, a regulator of cathepsins maturation. *Cell. Signal.* **26,** 716–723 (2014).
40. Peinado, H. *et al.* Melanoma exosomes educate bone marrow progenitor cells toward a pro-metastatic phenotype through MET. *Nat. Med.* **18,** 883–891 (2012).
41. Xiao, D. *et al.* Identifying mRNA, microRNA and protein profiles of melanoma exosomes. *PLoS ONE* **7,** e46874 (2012).
42. Lu, Y. J. *et al.* A molecular fluorescent dye for specific staining and imaging of RNA in live cells: a novel ligand integration from classical thiazole orange and styryl compounds. *Chem. Commun. (Camb)* **51,** 15241–15244 (2015).
43. Sun, V., Zhou, W., Majid, S., Kashani-Sabet, M. & Dar, A. MicroRNA-mediated regulation of melanoma. *Br. J. Dermatol.* **171,** 234–241 (2014).
44. Leibowitz-Amit, R., Sidi, Y. & Avni, D. Aberrations in the micro-RNA biogenesis machinery and the emerging roles of micro-RNAs in the pathogenesis of cutaneous malignant melanoma. *Pigment Cell Melanoma Res.* **25,** 740–757 (2012).
45. Zhao, F. *et al.* Activation of p38 mitogen-activated protein kinase drives dendritic cells to become tolerogenic in ret transgenic mice spontaneously developing melanoma. *Clin. Cancer Res.* **15,** 4382–4390 (2009).
46. Hankins, G. R. *et al.* M6P/IGF2 receptor: a candidate breast tumor suppressor gene. *Oncogene* **12,** 2003–2009 (1996).
47. Oates, A. J. *et al.* The mannose 6-phosphate/insulin-like growth factor 2 receptor (M6P/IGF2R), a putative breast tumor suppressor gene. *Breast Cancer Res. Treat.* **47,** 269–281 (1998).
48. Chappell, S., Walsh, T., Walker, R. & Shaw, J. Loss of heterozygosity at the mannose 6-phosphate insulin-like growth factor 2 receptor gene correlates with poor differentiation in early breast carcinomas. *Br. J. Cancer* **76,** 1558 (1997).
49. Gemma, A. *et al.* Mutation analysis of the gene encoding the human mannose 6-phosphate/insulin-like growth factor 2 receptor (M6P/IGF2R) in human cell lines resistant to growth inhibition by transforming growth factor β 1 (TGF-β 1). *Lung Cancer* **30,** 91–98 (2000).
50. Aprelikova, O. *et al.* The role of miR-31 and its target gene SATB2 in cancer-associated fibroblasts. *Cell Cycle* **9,** 4387–4398 (2010).
51. Golan, T. *et al.* Interactions of melanoma cells with distal keratinocytes trigger metastasis via notch signaling inhibition of MITF. *Mol. Cell* (2015).
52. Bell, R. E. *et al.* Transcription factor/microRNA axis blocks melanoma invasion program by miR-211 targeting NUAK1. *J. Invest. Dermatol.* **134,** 441–451 (2014).
53. Soderberg, A., Barral, A. M., Soderstrom, M., Sander, B. & Rosen, A. Redox-signaling transmitted in trans to neighboring cells by melanoma-derived TNF-containing exosomes. *Free Radic. Biol. Med.* **43,** 90–99 (2007).
54. Gu, J. *et al.* Gastric cancer exosomes trigger differentiation of umbilical cord derived mesenchymal stem cells to carcinoma-associated fibroblasts through TGF-β/Smad pathway. *PLoS ONE* **7,** e52465 (2012).
55. van den Boorn, J. G. *et al.* Skin-depigmenting agent monobenzone induces potent T-cell autoimmunity toward pigmented cells by tyrosinase haptenation and melanosome autophagy. *J. Invest. Dermatol.* **131,** 1240–1251 (2011).
56. Pinner, S. *et al.* Intravital imaging reveals transient changes in pigment production and Brn2 expression during metastatic melanoma dissemination. *Cancer Res.* **69,** 7969–7977 (2009).

METHODS

Cell culture. MNT-1, NIH/3T3, B16F10, HaCat, WM3682, WM3526 and WM3314 cells and primary human dermal fibroblasts (fibroblasts isolated from eyelid, adult donor; PromoCell) were cultured in DMEM medium (Biological Industries) supplemented with 10% FBS, 1% penicillin–streptomycin and 1% L-glutamine. The melanoma cell line MNT-1 was provided by V. Hearing (National Institutes of Health (NIH), Washington, USA). The melanoma cell lines WM3682, WM3526 and WM3314 were provided by L. Garraway (Harvard University, Cambridge, USA). Additionally, primary human dermal fibroblasts were isolated as previously described[51] and plated onto collagen dishes. Primary human melanocytes were isolated and grown from neonatal foreskins as described previously[14].

All cells were regularly tested for the absence of mycoplasma. No cell lines used in this study were found in the database of commonly misidentified cell lines that is maintained by ICLAC and NCBI Biosample. The cell lines were not authenticated. All experiments involving human samples have been approved by the E. Wolfson Medical Center, Israel (Helsinki Ethical approval no. 0015-16-WOMC) and the Sheba Medical Center, Israel (no. 9943). All tissues (paraffin blocks) used in this research were obtained from the archive of the pathological institute in Sheba and Wolfson medical centres. As the tissues were de-identified and coded the IRB approved their use without a consent form. Additionally, since our research included protein (immunologist) or microRNA (*in situ*) analysis without any genetic use whatsoever, the IRB approved the use of the tissues without a consent form.

Isolation of melanosomes from cell homogenates. Melanosomes from MNT-1 cells, primary normal melanocytes and B16F10 cells were isolated as described previously[3]. Briefly, cells were lysed in a glass homogenizer, and the lysate was separated by density sucrose gradients. To confirm that the RNA was confined inside the melanosomes, melanosomes were treated with 0.4 $\mu g\,\mu l^{-1}$ RNase (Fermentas) for 10 min at 37 °C; 10 U ml^{-1} RNase inhibitor (Fermentas) was then added. For WM3314 melanosomes isolation, cells stably expressed tyrosinase fused with mCherry. Cells were lysed in a glass homogenizer; lysate was filtered through a 0.45-μm filter and the filtrate was centrifuged at 20,000*g* for 1 h.

Isolation of vesicles from medium. Exosomes were isolated by differential ultracentrifugation as described previously[57]. To isolate melanosomes from the medium, the conditioned medium was centrifuged at 300*g* for 15 min and at 1,000*g* for 30 min, before melanosomes were pelleted by a centrifugation at 20,000*g* for 60 min (ref. 58). For the analysis of the whole spectrum of secreted vesicles, the conditioned medium was centrifuged at 300*g* for 15 min and then at 110,000*g* for 90 min.

Electron microscopy. Melanosomes were fixed with Karnovsky's fixative and then processed as previously described[59]. After dehydration in a series of increasing ethanol concentrations, samples were embedded in araldite. Embedded pellets were sectioned with a diamond knife on an LKB 3 microtome, and ultrathin sections (80 nm) were collected onto 200-mesh, thin bar copper grids. The sections on grids were sequentially stained with uranyl acetate and lead citrate for 10 min each and viewed with a Tecnai TEM 100 kV (Phillips) equipped with a MegaView II CCD (charge-coupled device) camera and Analysis version 3.0 software (SoftImaging System). Electron microscopy for exosomes, secreted melanosomes and the whole spectrum of secreted vesicles in medium was performed using two approaches: for negative staining, particles were adsorbed from suspension onto carbon-coated formvar grids and embedded in a thin film of uranyl acetate–methylcellulose (0.5% uranyl acetate (Merck) in 0.5% methylcellulose, 25 centipoise (Sigma)). For analysis of ultrathin sections, pellets were sequentially fixed in buffered aldehyde (4% formaldehyde/1% glutaraldehyde), osmium and ethanolic uranyl following embedding in epoxide (Sigma) according to standard procedures. Ultrathin sections of nominal thickness (50 nm) were post-stained with uranyl and lead. Images were taken with a ZEISS EM 912 transmission electron microscope equipped with a Proscan CCD camera (TRS).

Tyrosinase activity. Whole-cell or melanosome pellets were subjected to catechol and ascorbic acid solution. Tyrosinase activity assay was monitored by analysis of the absorbance decrease of the ascorbic acid peak at 265 nm wavelength[60].

Immunofluorescence. Fibroblasts were fixed with 4% paraformaldehyde for 20 min, stained with HMB-45 (Dako) and GPNMB (R&D) antibodies, followed by incubation with Alexa-488- or Alexa-594-conjugated secondary antibodies. Images were obtained at ×40 magnification using fluorescence microscopy (Nikon). For immunofluorescence of cells sorted from mouse tissue, cells were fixed with methanol, smeared on cover glasses and stained with p-ERK (Sigma-Aldrich) and IGF2R (Santa Cruz) antibodies. Immunostaining of formalin-fixed, paraffin-embedded tissues was performed as previously described[51]. Slides were incubated with FSP-1 (Abcam), HMB-45 (Dako), CD68 (Cell Marque), DCT (Abgent), IGF2R (Santa Cruz and Sigma-Aldrich) and GPNMB (R&D) antibodies. Staining was performed by incubating with Alexa-488- or Alexa-594-conjugated secondary antibodies. Images were obtained at ×20 or ×40 magnification using fluorescence microscopy (Nikon) or at ×63 magnification using Leica SP5 confocal microscopy. Catalogue numbers and dilutions of all antibodies used are shown in Supplementary Table 9.

RNA labelling. To visualize newly synthesized RNA in melanosomes, SYTO RNAselect (500 nM 20 min) (Life Technologies) was used. MNT-1 cells were stably transfected with a plasmid encoding a tyrosinase–mCherry and were incubated with RNAselect, washed and homogenized after 4 h. Melanosomes were analysed by FACS analysis. Events were acquired using FACS ARIA. The MNT-1 medium was collected and added to fibroblasts. After 12 h incubation, the fibroblasts were analysed by FACS or visualized using fluorescence microscopy (×100).

RNA purification and qRT-PCR. Total RNA was purified using Trizol (Invitrogen) according to the manufacturer's instructions, followed by DNase treatment (QIAGEN) and quantified by $OD_{260\,nm}/OD_{280\,nm}$ measurement. Mature miR-211, miR-320c, miR-149, miR-23, miR-let7a and miR-let7b were quantified using 10 ng of total RNA by TaqMan assay according to the manufacturer's protocols (Applied Biosystems). Expression level normalized to *RNU6B* expression. All experiments were performed at least in triplicates. Standard errors of the means (s.e.m.) are presented. qRT-PCR analysis of IL1-β, IL-6, IL-8, CXCL1 and other genes was performed as previously described[51]. Relative expression was normalized to GAPDH. All primers and oligonucleotide sequences used are shown in Supplementary Table 7.

MicroRNA microarray. Total RNA was isolated from the melanoma cell lines MNT-1, WM3314, melanosomes and exosomes using Trizol (Invitrogen) or the miRNeasy Mini Kit (Qiagen) according to the manufacturer's instructions. RNA was analysed on the Agilent 2100 Bioanalyzer (Agilent Technologies), and RNA concentrations were determined using a NanoDrop spectrophotometer. The RNA samples were analysed on the Agilent Human miRNA Microarray Release 19.0 or 21.0 in the Genomics and Proteomics Core Facility of DKFZ according to the manufacturers' recommendations. Briefly, fluorescently labelled miRNA was prepared according to the Agilent miRNA Complete Labeling and Hyb Kit protocol. Hybridization was performed in a SureHyb chamber (Agilent Technologies) at 55 °C for 20 h. Microarrays were scanned using the Agilent Scanner G2505C. The data were processed using R/Bioconductor scripts[9]. After quantile normalization, fold changes were calculated on the basis of mean values of the replicates. For further analysis, the 100 most highly enriched miRNAs in mature melanosomes compared with pre-mature melanosomes were evaluated for overlap with miRNAs previously associated with melanoma.

Expression profiling. Total RNA from melanosome-treated or untreated fibroblasts was isolated using Trizol (Invitrogen). Mature melanosomes used for the treatment were isolated from MNT-1 cell homogenates as described above. RNA quality was analysed on the Agilent 2100 Bioanalyzer (Agilent Technologies), and RNA concentrations were determined using the NanoDrop system. RNA from three replicates each was analysed on the Illumina Human Sentrix-12v4 BeadChip array by the Genomics and Proteomics Core Facility of DKFZ. Briefly, the Illumina Total Prep RNA Amplification Kit was used to synthesize first- and second-strand cDNA and for amplifying biotinylated cRNA. Hybridization was performed at 58 °C in GEX-HCB buffer (Illumina) at a concentration of 100 ng cRNA μl^{-1}, unsealed in a humidified chamber for 20 h. After washing and blocking, array signals were developed by a 10-min incubation in a 1 $\mu g\,ml^{-1}$ Cy3–streptavidin (Amersham Biosciences) and 1% blocking solution. Microarray scanning was performed in an iScan array scanner. The data were processed using R/Bioconductor scripts[61]. After quantile normalization, fold changes between melanosome-treated and untreated fibroblasts were calculated on the basis of mean values of the replicates.

Total RNA from fibroblasts transfected with miR-211, miR-320c or scrambled miR as control was isolated using Trizol (Invitrogen). RNA from two replicates each was analysed on Affymetrix Human Gene 1.1 ST Arrays. The data were processed using the Chipster microarray data analysis software (http://chipster.csc.fi)[62]. After RMA normalization and $\log_2$-transformation of expression values, fold changes for miR-211- and miR-320c-transfected fibroblasts versus control fibroblasts were calculated on the basis of mean values of the replicates.

Ingenuity Pathway Analysis. Computational analyses for the 10% most differentially expressed genes in treated fibroblasts compared with controls were performed using IPA software (Qiagen). Expression profiling data were sorted by the absolute value of the $\log_2$-transformed fold change, and the top 10% most differentially expressed genes were uploaded to IPA. Downstream Effects Analyses were performed with focus on cellular functions. These analyses provided predictions about the activation

DOI: 10.1038/ncb3399

state of each function, calculated as activation z-scores ($|z| > 2$ is considered significant)[63]. To analyse IGF1R downstream signalling, a computational network was generated showing all genes downstream of IGF1R from the Ingenuity Knowledge Base (for human species only) that are related to proliferation and migration of fibroblasts. This network was overlaid with the expression data of miR-211-transfected fibroblasts. In addition, the IPA canonical pathway for IGF1R was overlaid with expression profiling data of miR-211-transfected and melanosome-treated fibroblasts.

miRNA/mRNA correlation analysis. Paired miRNA/mRNA expression data were generated as described previously[52]. The correlation between MITF expression and each miRNA was calculated using Pearson's coefficient.

Transfection and luciferase reporter assay. NIH/3T3 cells were co-transfected with a luciferase construct and a miR-211 or empty vector. The luciferase reporter constructs contained either the wild-type (WT) form or a mutated version (mut) of the miR-211-binding site in the 3′UTR of *IGF2R*. Transfection was performed using jetPEI kit (Polyplus-transfection) according to the manufacturer's instructions. NIH/3T3 cells were treated with melanosomes after 24 h. Luciferase activities were determined using the Dual Luciferase kit (Promega) according to the manufacturer's recommendations. Results were normalized to the constitutively expressed *Renilla* luciferase.

Oligonucleotide transfection. miR-211 mimic, miR-320c mimic, control miRNA mimic, anti-miR-211 or control siRNA was transfected into fibroblast cells using HiPerFect (QIAGEN) according to the manufacturer's protocols. Cells were transfected twice with 100 pmol of oligonucleotides per well in 24 h intervals. Transfected cells were assayed 2 h after the second transfection.

Gel electrophoresis and immunoblotting. Fibroblast cells were lysed as previously described[51]. Membrane was exposed overnight to antibodies targeting phospho-ERK, total ERK, phospho-IGF1R and total-IGF1R (all from Cell Signaling). Proteins were visualized with SuperSignal Chemiluminescent Substrates (Pierce) using horseradish peroxidase-conjugated anti-mouse or anti-rabbit secondary antibody (Cell Signaling). Extraction of proteins from MNT-1 whole cells and cytoplasm, melanosomes isolated from MNT-1 cell homogenates and exosomes was performed using an optimized lysis buffer[64]. Proteins were incubated overnight with antibodies targeting tyrosinase (Santa Cruz), DCT (Abgent), GPNMB (R&D), CD63 (Abgent), α-enolase (Abgent), HSC70 (Santa Cruz) and Rab27a (Santa Cruz). After incubating with horseradish peroxidase-conjugated secondary antibodies (anti-mouse and anti-rabbit: Vector, anti-goat: Santa Cruz), proteins were detected using Amersham ECL Prime Western Blotting Detection Reagent (GE Healthcare). Catalogue numbers and dilutions of all antibodies used are shown in Supplementary Table 9. Unprocessed original scans of western blots are in Supplementary Fig. 7.

Proliferation assay. Cell proliferation was measured by crystal violet staining as previously described[12]. Optical absorbance measured at 595 nm was assumed to be proportional to the number of viable cells in each well.

Scratch assay. Fibroblasts were seeded into 24-well plates. The confluent cell monolayers were wounded by manually drawing a gap with a plastic pipette tip. The ability of cells to migrate into the cleared section was monitored by live image microscopy at the specific time points.

Contractility assay. A fibroblast contraction assay was performed according to a published method[65]. Fibroblasts were trypsinized and mixed with type I collagen from rat tail tendon (BD Bioscience) adjusted to a final value of 2.5 mg ml^{-1} with 0.01% acetic acid, 10× DMEM, and 0.1 N NaOH. Fibroblasts (2.5×10^5 cells ml^{-1} final concentration) were suspended in collagen (1.25 mg ml^{-1} of collagen final concentration), aliquoted into 24-well plates (300 µl per well), and incubated at 37 °C for 60 min to allow collagen polymerization, followed by the addition of DMEM-containing 10% FBS (300 µl). To initiate collagen gel contraction, polymerized gels were gently released from the underlying DMEM. The collagen gels containing cells were incubated at 37 °C overnight, and the diameters of the collagen gels were measured.

Invasion. Approximately 5×10^5 melanoma cells were added in duplicate to invasion chambers coated with Matrigel (BD Biosciences). Invasion analysis was performed as previously described[51]. In all assays, ten fields per insert were photographed. The number of invaded cells was normalized to the number of total seeded cells.

***In situ* hybridization analysis.** Pathological paraffin-embedded tissues were fixed with 4% PFA, digested with proteinase K (NEB New England Biolabs) for 10 min at room temperature, and denatured at 80 °C. Hybridization was conducted overnight at 54 °C with digoxigenin-labelled probes of hsa-miR-211 (Exiqon). The slides were washed with TBST, blocked with 10% normal goat serum and incubated with sheep anti-digoxigenin antibody (Roche) in TBST for 1 h at room temperature, following treatment with Tyramide Signal Amplification (TSA) Systems (PerkinElmer).

Mouse melanoma model. All animal experiments were conducted with approval from the University of Tel Aviv Institutional Animal Care and Use Committee (M-11-053, 01-15-086; M-13-078). No statistical method was used to predetermine sample size, but the sample size was chosen to be adequate to receive significant results (P value < 0.05). The experiments were not randomized and the investigators were not blinded to allocation during experiments and outcome assessment. Primary fibroblasts were treated with melanosomes or PBS for 48 h, and then co-cultured for 48 h with 50,000 WM3526 melanoma cells stably expressing mCherry and luciferase reporter. Co-cultured cells were mixed with Growth Factor Reduced Matrigel (BD Biosciences) and injected subcutaneously into the dorsal site of NOD–SCID–IL2γ-null mice (NSG, The Jackson Laboratory) at the age of 8 weeks. At 14 days post injection, the tumour size was assessed by bioluminescence imaging after injection of 150 µl luciferin (Promega) using an IVIS Spectrum system (Caliper Life Sciences, PerkinElmer). A total of 24 mice were used, 12 control fibroblasts, 12 melanosome-treated fibroblasts; in each group 6 males and 6 females.

***In vivo* Matrigel assays.** Approximately 5×10^5 RMS cells in 25 µl PBS were mixed with 25 µl Growth Factor Reduced Matrigel (BD Biosciences) and injected subdermally into the dorsal area of C57BL/6 male mice (7 weeks old). After 14 days, tumours and tumour-associated stroma were harvested and digested into single-cell suspensions. Control fibroblasts were taken from mouse ears. For Fig. 5i: 12 mice were injected with melanoma and 4 mice were used as control.

For Fig. 7a: 20 mice were injected with melanoma; ears from these mice were used as control.

FACS sorter. Cell sorting was carried out as previously published[23]. Fibroblasts were sorted using FITC-conjugated PDGFRα. PERCP-conjugated CD11b or CD45 was used to exclude macrophage cell contamination. Melanoma cells stably expressing mCherry were sorted using the mCherry filter.

FACS analysis. MNT-1 cells, secreted exosomes and secreted melanosomes were labelled with anti-human-CD81–PE (BD Biosciences) and anti-human-CD63–PE (Beckman Coulter). The labelling was performed at 4 °C using PBS containing 1% FBS during 30 min. Events were acquired using a FACS CANTO and analysed using FACS Diva (version 6.1.3) followed by FlowJo (version X.0.7).

Melanin and protein quantification of melanosomes. To generate standard curves for the correlation between melanosome number and melanin or protein concentration, melanosomes were isolated from melanoma cell homogenates and quantified by nanoparticle tracking analysis (NTA), using a NanoSight LM10 equipped with a 405 nm laser (Malvern Instruments). Data were analysed with the NTA 3.0 software. Melanosome stocks were diluted with PBS to a concentration between 10^8 and 10^9 particles ml^{-1}. Each sample was analysed five times for 60 s; the mean values were used for further calculations. From the melanosome stock, aliquots of different volumes from 1 to 100 µl were taken. For each aliquot the number of melanosomes was calculated on the basis of the concentration of the melanosome stock and the melanin and protein concentrations were measured. Melanin content was assessed as described previously[66]. The melanosome aliquots were centrifuged at 5,000*g* for 20 min at 4 °C, pellets were resuspended in 500 µl of 1 M NaOH in 10% DMSO and incubated at 80 °C for 2 h. After centrifugation at 5,000*g* for 20 min, the melanin concentration of the supernatants was determined by measuring the absorbance at 420 nm. A standard curve was generated with synthetic melanin (MP Biomedicals) for the range of 1.25–100 µg ml^{-1}. To determine the protein content, 50 µl of lysis buffer was added to each melanosome aliquot. After incubation on ice for 2 h, lysates were centrifuged for 20 min at 18,000*g* at 4 °C and the protein concentration of the resulting supernatants was determined using a BCA Protein Assay kit (Thermo Scientific). A standard curve was generated with Protein Standard (Sigma-Aldrich) for the range of 0.125–2 mg ml^{-1}.

Melanosome quantification in melanoma human sections. Images were taken using confocal microscopy (Leica SP8) and quantitatively analysed using ImageJ. An average number of 10 cells were taken from each field, with five fields analysed for each group. In each field the melanosome intensity and total intensity of the fibroblasts were measured. The total intensity of each fibroblast was divided by the average intensity of one melanosome to calculate the number of melanosomes in each cell.

IGF2R and miR-211 intensity in melanoma human sections. Images were taken using confocal microscopy (Leica SP8) and quantitatively analysed using ImageJ.

For each condition, 60 cells from each of three different patients were analysed. The intensity of each cell was measured and divided by the cell area to get the mean intensity per cell. Mean intensities for IGF2R and miR-211 were compared between normal and melanoma sections of the same patient.

Liposome preparation. Lissamine rhodamine B sulfonyl (16:0 Liss Rhod PE ,810158, Avanti Polar Lipids) liposomes (MW 1,249.641) were prepared by an ethanol injection method[67]. Liposomes were composed of Liss Rhod PE, hydrogenated soybean phosphatidylcholine (HSPC) (Lipoid, MW 762 g mol^{-1}), cholesterol (Sigma-Aldrich, MW 386.65 g mol^{-1}), and polyethylene glycol distearoyl phosphoethanolamine (m2000PEG –DSPE; Lipoid, MW 2,805 g mol^{-1}). The loading concentration of the lipid was 50 mM in PBS. To achieve 500-nm vesicles, lipids were dissolved in pure ethanol, warmed to 65 °C and added to the PBS. The liposomes were passed through an extruder (Northern Lipids) at 60 °C through polycarbonate membrane filters (Whatman) of 800, and 400 nm. Five extrusion steps were applied per filter type. After extrusion, size was measured using dynamic light scattering (ZetaSizer ZSP, Malvern Instruments). The polydispersity index was 0.6, and average particle size was 405 nm. The liposome concentration was measured using the NanoSight NS300 (Malvern Instruments) and was 4.25×10^{11} particles ml^{-1}. Supplementary Video 1 shows a video of these liposomes.

Liposome standard curve and liposome cellular quantification. Rhodamine-labelled liposomes were added to PBS. Samples were monitored using a SpectraMax M5e HTRF (Molecular Devices) with excitation at 584 nm and emission at 612 nm. Primary fibroblasts were treated with 500 liposomes per cell for 24 h, washed five times and harvested. Cells were counted using Countess (Invitrogen) and fluorescence intensity was quantified.

Analysis of secreted vesicle concentration. Samples were scanned three times for the duration of 60 s, to provide statistically significant data, using the Nanosight NS300, equipped with a green laser (532 nm). To determine secreted exosome (70–100 nm) and melanosome (200–600 nm) concentrations, each population was measured in a different size path.

Reagents. MAPK inhibitor, U0126 (Cell Signaling), was dissolved in DMSO. Vehicle was added to controls and U0126 (final concentrations 10 μM) was added for the whole period of the respective experiment. Melanosome inhibitor, SB202190 (Sigma-Aldrich), dissolved in DMSO, was added to the cells (final concentrations 20 μM) for 24 h followed by a 24 h wash. Mitomycin-c dissolved in H_2O was added to the cells (final concentrations 10 μg ml^{-1}) for 2 h, followed by a wash with PBS.

Statistics and reproducibility. Standard parametric *t*-tests were applied and standard errors were calculated for each data set with $n > 2$. Variations with P values < 0.05 were considered significant. Statistics source data are provided in Supplementary Table 8.

The human melanoma images shown in Fig. 1 and Supplementary Figs 1 and 2 are from 11 individual patients; images in Fig. 5h and Supplementary Fig. 6e represent two patients; and images in Fig. 7c and Supplementary Fig. 7c–f are from five individuals. The electron microscopy images in Fig. 2a,b and Supplementary Figs 3c and 4i,j are representative of three independent experiments. Immunofluorescent staining depicted in representative images Figs 2c and 7b and Supplementary Figs 3g, 4n and 6h was performed in three independent experiments. Fluorescent images in Figs 2o and 4a and Supplementary Figs 4f and 7g represent three independent experiments, Supplementary Fig. 4h results from one experiment. The bright-field microscopy images in Supplementary Fig. 4o resulted from three independent experiments. The immunoblot in Fig. 6e represents two independent experiments; the immunoblots in Fig. 6f and Supplementary Fig. 3b,e were performed once. Scratch assays were done twice (Figs 2j,l and 6g and Supplementary Fig. 4b,q) or three times (Figs 2f and 5c,f and Supplementary Figs 3i and 6b), and collagen contraction assays three (Fig. 5d and Supplementary Fig. 6c) or four (Fig. 2g) times. FACS analyses were performed once (Fig. 3c and Supplementary Figs 3d and 4k) or twice (Fig. 4b). NanoSight analysis in Supplementary Fig. 4a occurred in three independent experiments. Standard curves are based on one (Supplementary Fig. 3h: melanosome number based on protein concentration; Supplementary Fig. 4g) or two (Supplementary Fig. 3h: melanosome number based on melanin concentration) independent experiments. Images in Fig. 3a,b are representative of two independent experiments.

Data availability. miRNA microarray data and mRNA profiling data in support of this study have been deposited at the Gene Expression Omnibus (GEO) with primary accession number: GSE72620.

SubSeries linked to GSE72620: GSE72229; GSE72337; GSE72619; GSE79411.

Statistics source data for Figs 2 and 4–7, and Supplementary Figs 3 and 4–7 have been provided as Supplementary Table 8. All other data supporting the findings of this study are available from the corresponding author on request.

57. Lazar, I. *et al.* Proteome characterization of melanoma exosomes reveals a specific signature for metastatic cell lines. *Pigment Cell Melanoma Res.* **28,** 464–475 (2015).
58. D'Souza-Schorey, C. & Clancy, J. W. Tumor-derived microvesicles: shedding light on novel microenvironment modulators and prospective cancer biomarkers. *Genes Dev.* **26,** 1287–1299 (2012).
59. Morris, J. K. A formaldehyde glutaraldehyde fixative of high osmolality for use in electron microscopy. *J. Cell Biol.* **27,** 137–139 (1965).
60. Ros, J. R., Rodriguez-Lopez, J. N. & Garcia-Canovas, F. Effect of L-ascorbic acid on the monophenolase activity of tyrosinase. *Biochem. J.* **295,** 309–312 (1993).
61. Ritchie, M. E., Dunning, M. J., Smith, M. L., Shi, W. & Lynch, A. G. BeadArray expression analysis using bioconductor. *PLoS Comput. Biol.* **7,** e1002276 (2011).
62. Kallio, M. A. *et al.* Chipster: user-friendly analysis software for microarray and other high-throughput data. *BMC Genomics* **12,** 507 (2011).
63. Kramer, A., Green, J., Pollard, J. Jr & Tugendreich, S. Causal analysis approaches in Ingenuity Pathway Analysis. *Bioinformatics* **30,** 523–530 (2014).
64. Alhamdani, M. S. *et al.* Single-step procedure for the isolation of proteins at near-native conditions from mammalian tissue for proteomic analysis on antibody microarrays. *J. Proteome Res.* **9,** 963–971 (2010).
65. Bogatkevich, G. S., Tourkina, E., Silver, R. M. & Ludwicka-Bradley, A. Thrombin differentiates normal lung fibroblasts to a myofibroblast phenotype via the proteolytically activated receptor-1 and a protein kinase C-dependent pathway. *J. Biol. Chem.* **276,** 45184–45192 (2001).
66. Magina, S. *et al.* Inhibition of basal and ultraviolet B-induced melanogenesis by cannabinoid CB(1) receptors: a keratinocyte-dependent effect. *Arch. Dermatol. Res.* **303,** 201–210 (2011).
67. Pons, M., Foradada, M. & Estelrich, J. Liposomes obtained by the ethanol injection method. *Int. J. Pharm.* **95,** 51–56 (1993).

nature cell biology

DOI: 10.1038/ncb3399

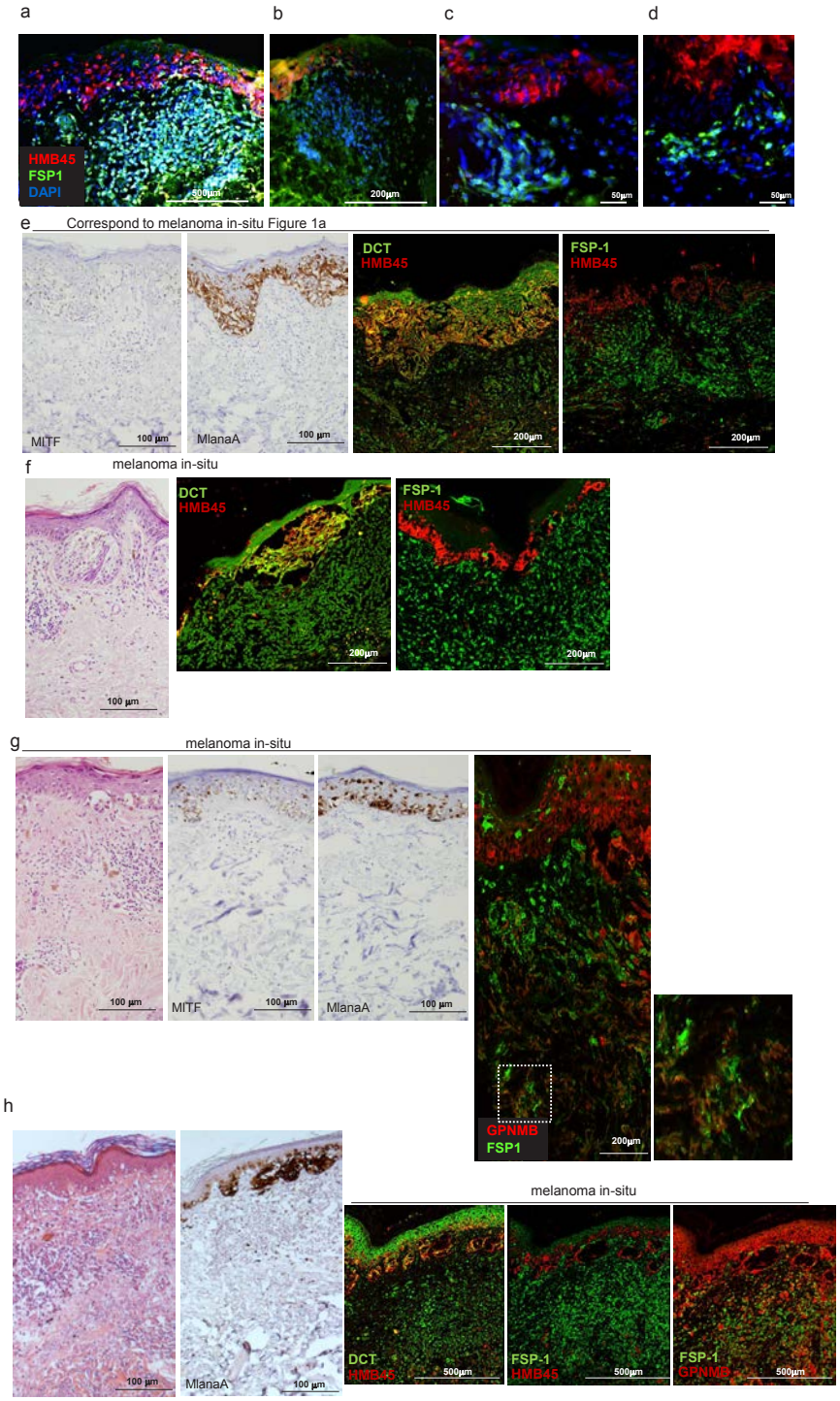

Supplementary Figure 1: Fibroblasts aggregation at a distance from melanoma regions contain melanoma particles. (a-d) Immunofluorescence analysis of sections from four melanoma patients. DAPI-stained nuclei appear in blue. (e) Left: Immunohistochemistry staining (20X magnification) of MITF and MelanA in *in situ* melanoma sample. Right: Immunofluorescence analysis (63X magnification) of DCT (green) and HMB-45 (red) or FSP-1 (green) and HMB-45 (red). (f) Left: H&E staining (20X magnification) of *in situ* melanoma. Right: Immunofluorescence analysis (63X magnification) of HMB-45 (red) and DCT (green) or FSP-1 (green). Yellow signal indicates co-localization. (g) Left: H&E staining, immunohistochemistry for MITF and MelanA for *in situ* melanoma (20X magnification). Right: Immunofluorescence analysis of GPNMB (red) and FSP-1 (green). Yellow signal indicates co-localization of FSP-1 and GPNMB (63X magnification), in dashed square higher magnification image (100x magnification). (h) From left to right in *in situ* melanoma: H&E staining, immunohistochemistry (20X magnification) for MelanA, immunofluorescence analysis of HMB-45 (red) and DCT (green), HMB-45 (red) and FSP-1 (green), GPNMB (red) and FSP-1 (green). Yellow signal indicates co-localization (63X magnification).

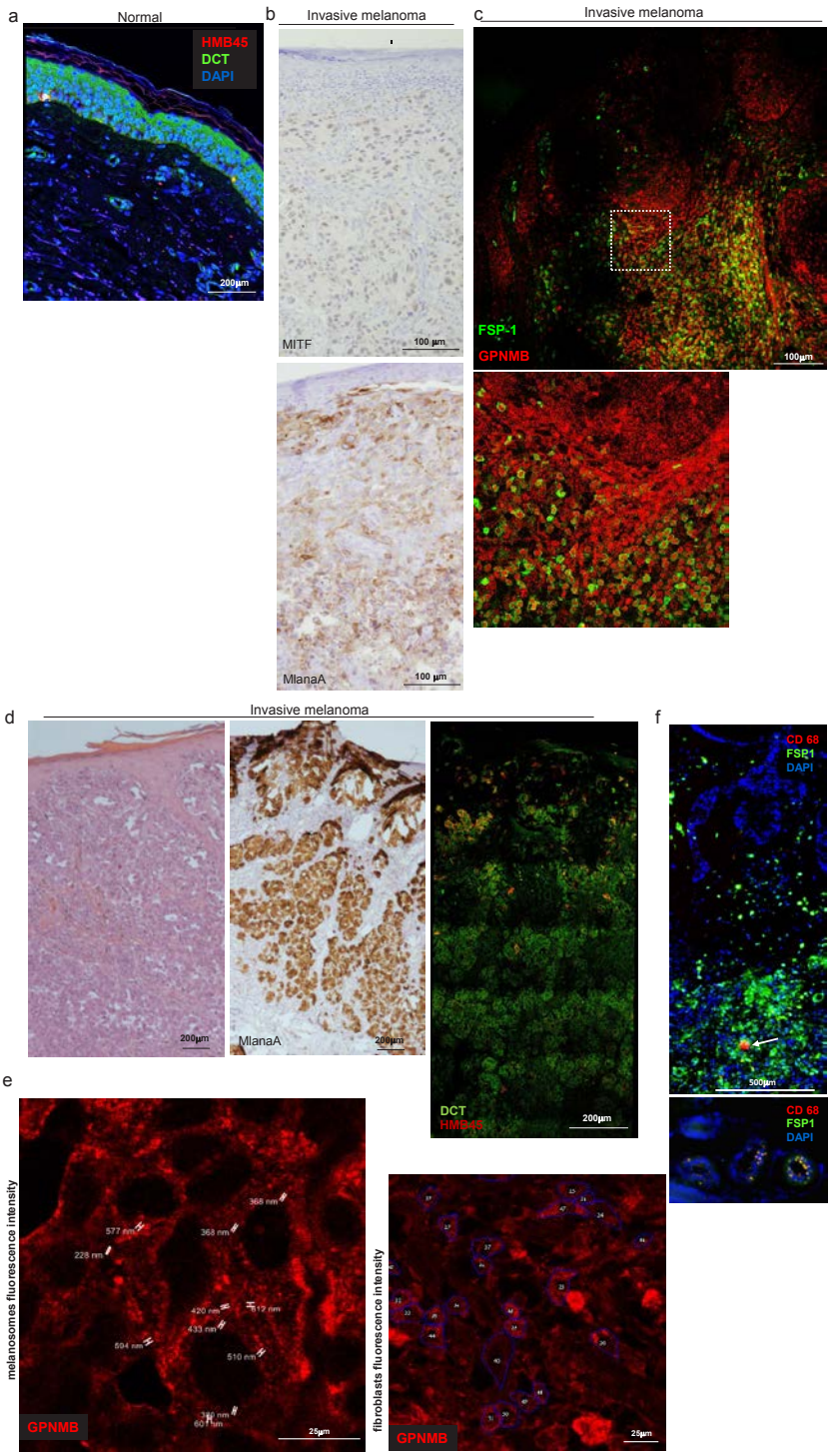

Supplementary Figure 2 Fibroblasts aggregation at a distance from melanoma regions contain melanoma particles. (a) Normal skin stained for HMB-45 (red) and DCT (green). DAPI-stained nuclei appear in blue (63X magnification). (b) Immunohistochemistry for MITF and MelanA for invasive melanoma (20X magnification) shown in Figure 1. (c) Immunofluorescence analysis of FSP-1 (green) and GPNMB (red) for invasive melanoma (20X magnification). Higher magnification image in the lower panel (100X magnification). (d) Left: H&E staining and immunohistochemistry for MelanA (20X magnification) for invasive melanoma. Right: Immunofluorescence analysis of DCT (green) and HMB-45 (red) for invasive melanoma (63X magnification). (e) Melanosome quantification method. Immunofluorescence analysis of dermal fibroblasts in superficial melanoma patient samples reveals staining for GPNMB (red) indicative of melanosomes. Left: Red fluorescence regions within fibroblast cytoplasm at the size of 300-600 nm are marked and were analyzed for fluorescence intensity (n=80 melanosomes). Right: Whole cell fibroblasts were marked and analyzed for fluorescence intensity (n=100 cells). (f) A single representative sample is shown stained for FSP1 (green) and macrophage marker CD68 (red). White arrow indicates non-specific staining, and yellow signal indicates co-localization of FSP-1 and CD68. DAPI-stained nuclei appear in blue.

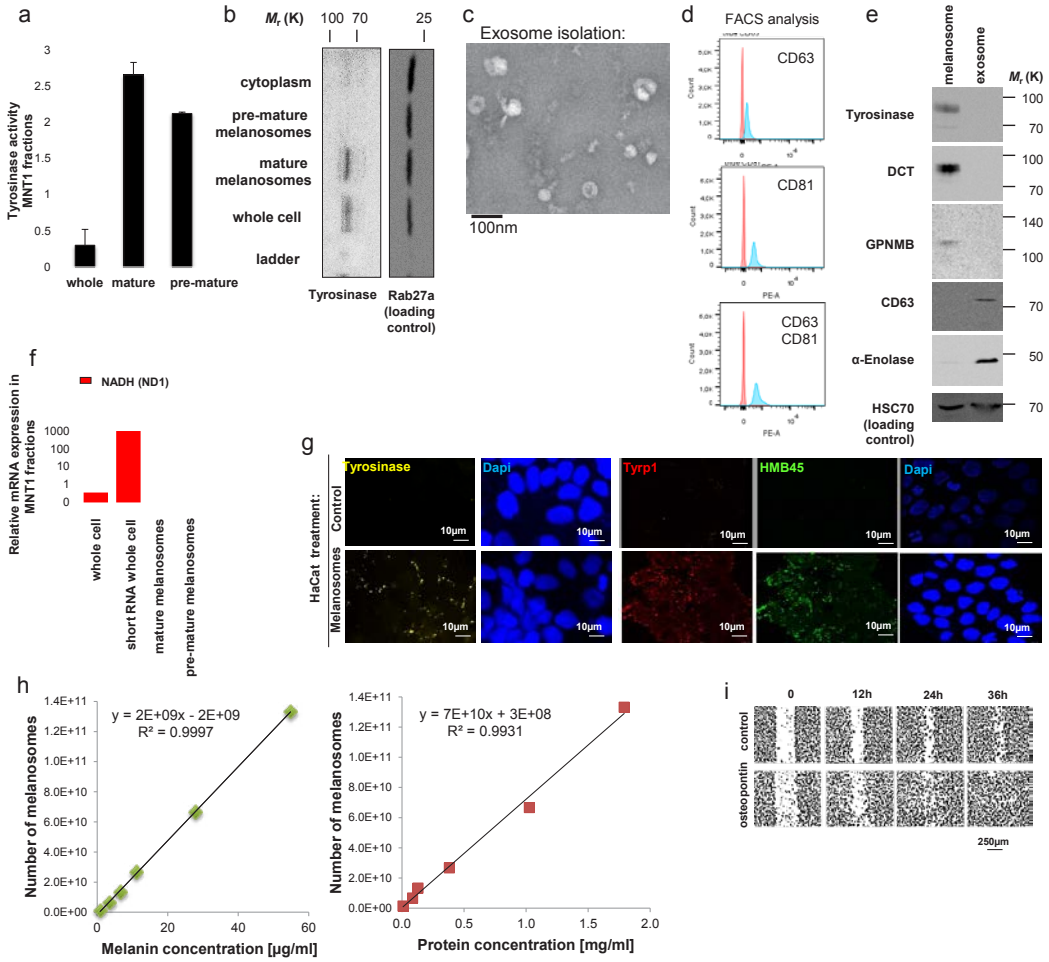

Supplementary Figure 3 Melanoma melanosomes transfer into fibroblasts leads to reprogramming. (a) Tyrosinase activity of MNT-1 whole cell extracts or isolated mature and pre-mature melanosomes. Values are normalized to total protein concentration. Error bars represent ± SEM, * indicates $p<0.05$ (n=5 independent experiments). (b) Tyrosinase protein levels in indicated fractions. Rab27a was analyzed as a loading control. (c) Electron microscopy analysis of exosomes. (d) Expression of CD63 and CD81 in exosomes purified from MNT-1 cells by FACS analysis. Upper panel shows the analysis of expression of CD63 (blue) compared to unstained exosomes (red). Middle panel shows the analysis of expression of CD81 (blue) compared to unstained exosomes (red). Lower panel shows the analysis of expression of exosome markers CD63 and CD81 (blue) compared to unstained exosomes (red). (e) Protein levels in melanosomes isolated from MNT-1 cell homogenates and exosomes isolated from MNT-1 conditioned medium. Hsc70 was used as a loading control. (f) ND-1 levels in indicated fractions, normalized to *GAPDH* (n=1 independent experiment). (g) Immunofluorescence staining of HaCat cells upon melanosome treatment. Melanosomal markers: tyrosinase, Tyrp1, and HMB-45 appear in yellow, red, and green, respectively. DAPI-stained nuclei appear blue. (h) Standard curves of melanosome number based on melanin and protein concentrations. (i) Fibroblasts migration upon osteopontin (400nM) treatment. Unprocessed scans of Western Blots are shown in Supplementary Fig. 8.

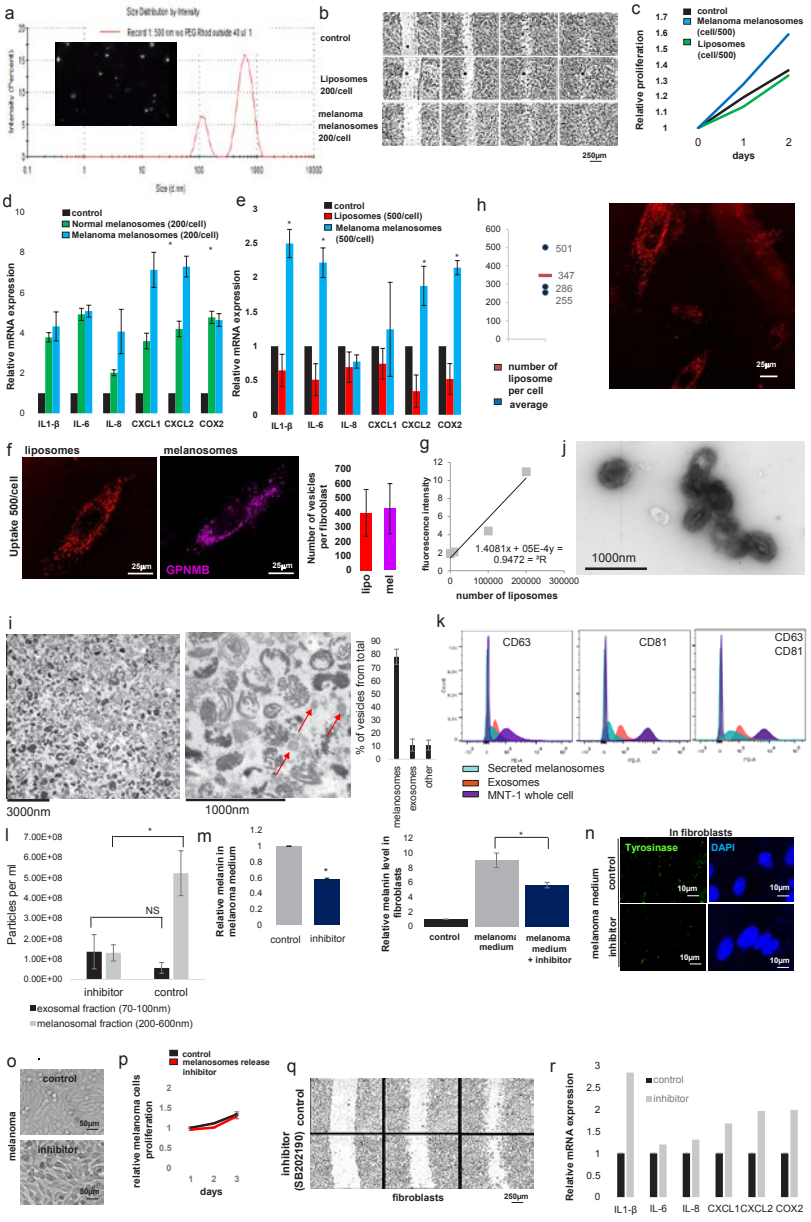

Supplementary Figure 4 Melanoma melanosomes transfer into fibroblasts leads to reprogramming. (a) Dynamic light scattering image of liposomes from a NanoSight analysis. Middle: Snapshot image of liposomes movie (Supplementary video 1). (b) Fibroblast migration upon indicated treatments. (c) Growth rate of fibroblasts upon indicated treatments (n=2 independent experiments). (d,e) The pro-inflammatory gene signature of CAFs upon indicated treatments. Data were normalized to *GAPDH* (n=3 independent experiments). (f) Left: Representative images of fibroblasts treated with 500 rhodamine-labeled liposomes or melanosomes (immunostained with GPNMB) per cell. Right: Average number of vesicles per cell (n=6 cells for each group, 2 independent experiments). (g) Standard curve of liposome number. (h) Left: Number of liposomes per cell, calculated based on the standard curve (n=3 measurements each of $9*10^3$ cells). Right: Representative image of fibroblasts treated with 500 rhodamine-labeled liposomes per cell. (i) Left: Electron microscopy analysis of secreted vesicles. Right: Higher magnification of the same sample. Red arrows indicate exosomes. Graphs: Percentages of indicated vesicles (n=3 individual experiments). (j) Electron microscopy analysis of secreted melanosomes. (k) FACS analysis of CD63 and CD81 expression in indicated vesicles. Unstained MNT-1 cells appear in pale purple, stained MNT-1 cells in purple, unstained MNT-1 exosomes in pale red, stained MNT-1 exosomes in red, unstained MNT-1 melanosomes in pale blue, and stained MNT-1 melanosomes in blue. (l) NanoSight analysis of the secreted vesicle population upon P38 inhibitor treatment (n=3 independent experiments). (m) Left: Melanin levels in melanoma medium upon SB202190 treatment. Data were normalized to RNU6B (n=4 independent experiments). Right: Melanin levels in fibroblasts treated with medium from melanoma cells incubated with or without SB202190. Fibroblast medium was used as a control. Values were normalized to total protein amount (n=8 samples, 3 independent experiments). (n) Immunostaining of fibroblasts treated with medium from melanoma cells that were pre-treated with SB202190. Tyrosinase is stained green; DAPI-stained nuclei appear in blue. (o) Bright field pictures of melanoma cells upon SB202190 treatment. (p) Growth rates of melanoma cells upon SB202190 treatment. (n=3 independent experiments). (q,r) Migration and pro-inflammatory gene signature of fibroblasts treated with SB202190. Data were normalized to *GAPDH* (n=2 independent experiments). In all relevant panels error bars represent ± SEM; * indicates $p<0.05$.

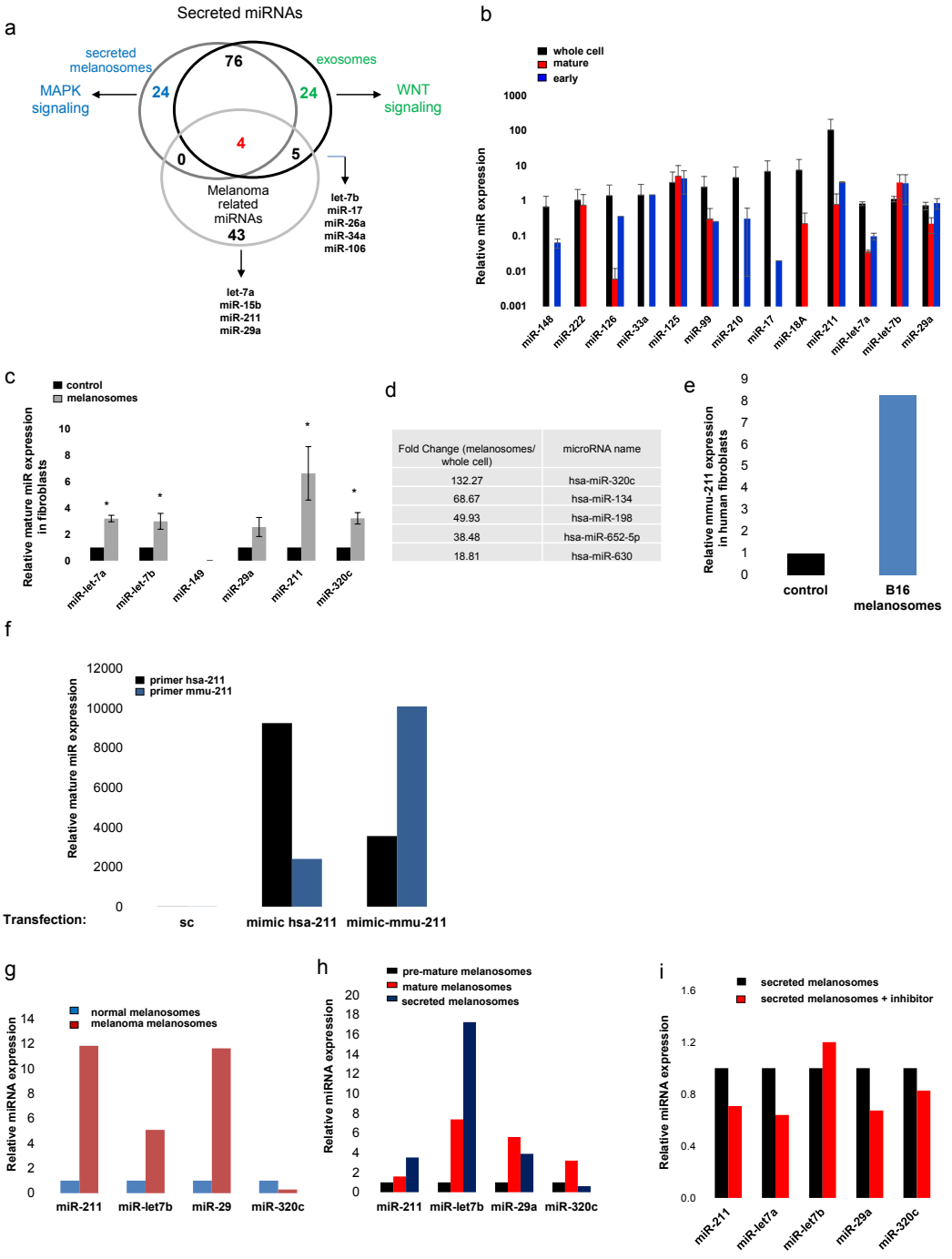

Supplementary Figure 5 Identification of melanosomal miRNAs and their trafficking into fibroblasts. (a) Venn diagram showing the overlap between the 100 most highly expressed miRNAs in melanosomes, exosomes and melanoma-related miRNAs (literature based 41,42). (b) Yield of mature miRNAs in preparations from whole cells, mature melanosomes, and early melanosomes. Data were normalized to levels of RNU6B. Error bars represent ± SEM (n=3 independent experiments). (c) Levels of indicated mature miRNAs were evaluated in fibroblasts treated with melanosomes or PBS (control) using RT-PCR. Data were normalized to RNU6B levels. Error bars represent ± SEM, * indicates $p<0.05$ (n=4 independent experiments). (d) Table of the five microRNAs that are most up-regulated in mature melanosomes compared to their levels in whole cells. (e) Expression level of mature mmu-miR-211 in human fibroblasts after treatment with B16F10 melanosomes was determined using qRT-PCR. Data were normalized to RNU6B (n=2 independent experiments). (f) Human primary fibroblasts were transfected with human or mouse miR-211 mimic (hsa and mmu, respectively). qRT- PCR analysis of both miRNAs. Data were normalized to RNU6B (n=2 independent experiments). (g) Mature miRNAs levels in normal and melanoma melanosomes (n=2 independent experiments). (h) Levels of mature miRNAs in indicated fractions (n=2 independent experiments). (i) Levels of mature miRNAs in secreted melanosomes treated with the inhibitor (SB202190), normalized to RNU6B (n=2 independent experiments).

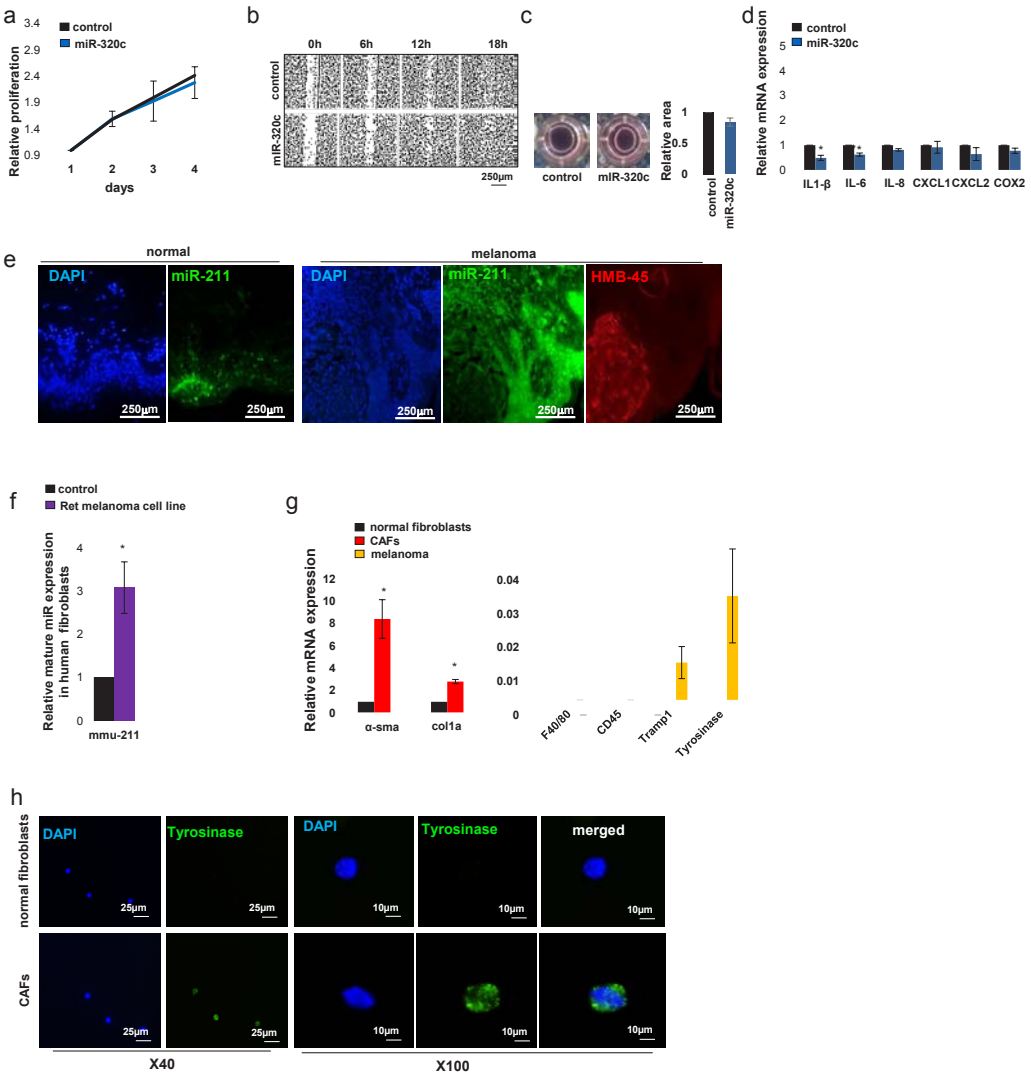

Supplementary Figure 6 Fibroblast reprogramming into CAFs is melanosomal miR-211 dependent. Fibroblasts treated with miR-320c were analyzed in comparison to control fibroblasts treated with scrambled miRs. The fibroblasts were subjected to the following analyses: (a) growth rate (error bars represent ± SEM, n=4 independent experiments); (b) migration tested by scratch assay; (c) fibroblast collagen remodeling capacity examined by three-dimensional collagen contraction assay (error bars represent ± SEM, n=5 independent experiments); and (d) pro-inflammatory gene expression levels tested by qRT-PCR normalized to *GAPDH* levels (error bars represent ± SEM, * indicates p<0.05, n=3 independent experiments). (e) *In situ* hybridization analysis (green, 20x magnification) of miR-211 expression levels in healthy skin sample (left) and sections from the skin of a melanoma patient (right). Immunofluorescence staining of HMB-45 of the same magnification and location (red). DAPI-stained nuclei appear blue. (f) Mature mouse miR-211 levels (mmu-miR-211) were measured in human fibroblasts that were treated with medium of Ret melanoma cell line or with control medium. Data were normalized to RNU6B levels. Error bars represent ± SEM, * indicates p<0.05 (n=3 independent experiments). (g) PDGFRα-positive fibroblasts from local tumor stroma and melanoma cells from tumor were assessed for the expression of fibroblast markers (α-SMA, collagen), macrophage markers (CD45, F40/80), and melanoma markers (trpm1, tyrosinase). Results were compared to the expression in normal fibroblasts sorted from mouse ears and normalized to GAPDH. Error bars represent ± SEM, * indicates p<0.05 (n=20 mice for treatment and 12 for control in 3 independent experiments). (h) Sorted fibroblasts from normal and stromal tissue stained for tyrosinase (green). DAPI-stained nuclei appear blue. Left panel: 40x magnification, right panel: 100x magnification.

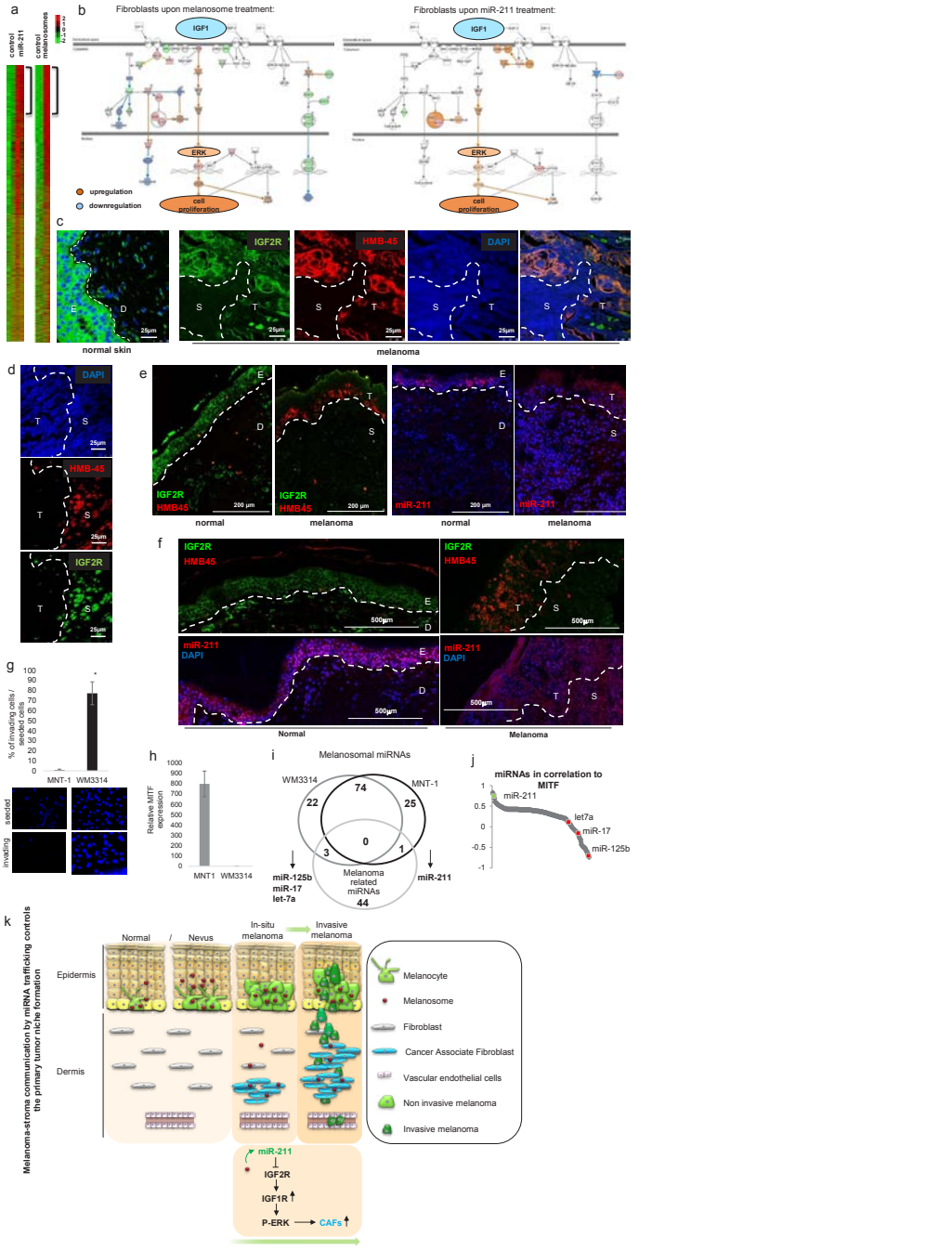

Supplementary Figure 7 Melanosomal miR-211 induces CAF formation via up-regulation of MAPK signaling. (a) Hierarchical clustering analysis of mRNA expression profiles of fibroblasts upon indicated treatments. Each row represents the mean of signal log ratios using a color-code scale. (b) Canonical pathway for IGF1R signaling in fibroblasts upon indicated treatments, generated with IPA. Gene expression levels are relative to control fibroblasts. Up- and down-regulated genes are labeled red or green, respectively; predicted activation is shown in orange, inhibition in blue. Lines represent known interactions. Orange arrows: activation; blue arrows: inhibition; yellow arrows: inconsistency between observation and prediction; grey arrows: lack of supporting data. (c,d) Immunostaining of HMB-45 and IGF2R in human specimens. Dashed lines separate tumor (T) and stroma (S); epidermis (E) and dermis (D) are indicated. DAPI-stained nuclei appear blue.. (e) Left: Immunostaining of HMB-45 and IGF2R in human specimens. Right: *In situ* hybridization of miR-211. Dashed lines separate tumor (T) and stroma (S); epidermis (E) and dermis (D) are indicated. DAPI-stained nuclei appear blue (63X magnification). (f) Top: Immunostaining of HMB-45 and IGF2R in human specimens. Bottom: *In situ* hybridization of miR-211. Dashed lines separate tumor (T) and stroma (S); epidermis (E) and dermis (D) are indicated. DAPI-stained nuclei appear blue (63X magnification). (g) MNT-1 and WM3314 melanoma cells invasion abilities, measured with a Matrigel invasion assay. Graph plots percent of invading cells. Representative images of invading and seeded cells are shown; DAPI-stained nuclei appear in blue. Error bars represent ± SEM, * indicates $p<0.05$ (n=3 independent experiments). (h) MITF expression levels in MNT-1 and WM3314 melanoma cells normalized to GAPDH. Error bars represent ± SEM (n=3 independent experiments). (i) Venn diagram showing the overlap between the 100 most highly expressed miRNAs in MNT-1 and WM3314 mature melanosomes and melanoma-related miRNAs (literature based[43,44]). (j) Pearson's correlation for the expression level of each miRNA relative to MITF in 11 melanoma cell lines. miR-211, Let7a, miR-17 and miR-125b are highlighted (correlations of $p < 0.05$). (k) A summary model - The formation of the melanoma primary niche by miRNA trafficking. Graphical model describing our findings which demonstrate that melanoma cells directly affect the formation of the dermal tumor niche by miRNA trafficking prior to invading the dermis.

Supplementary Figure 2b:

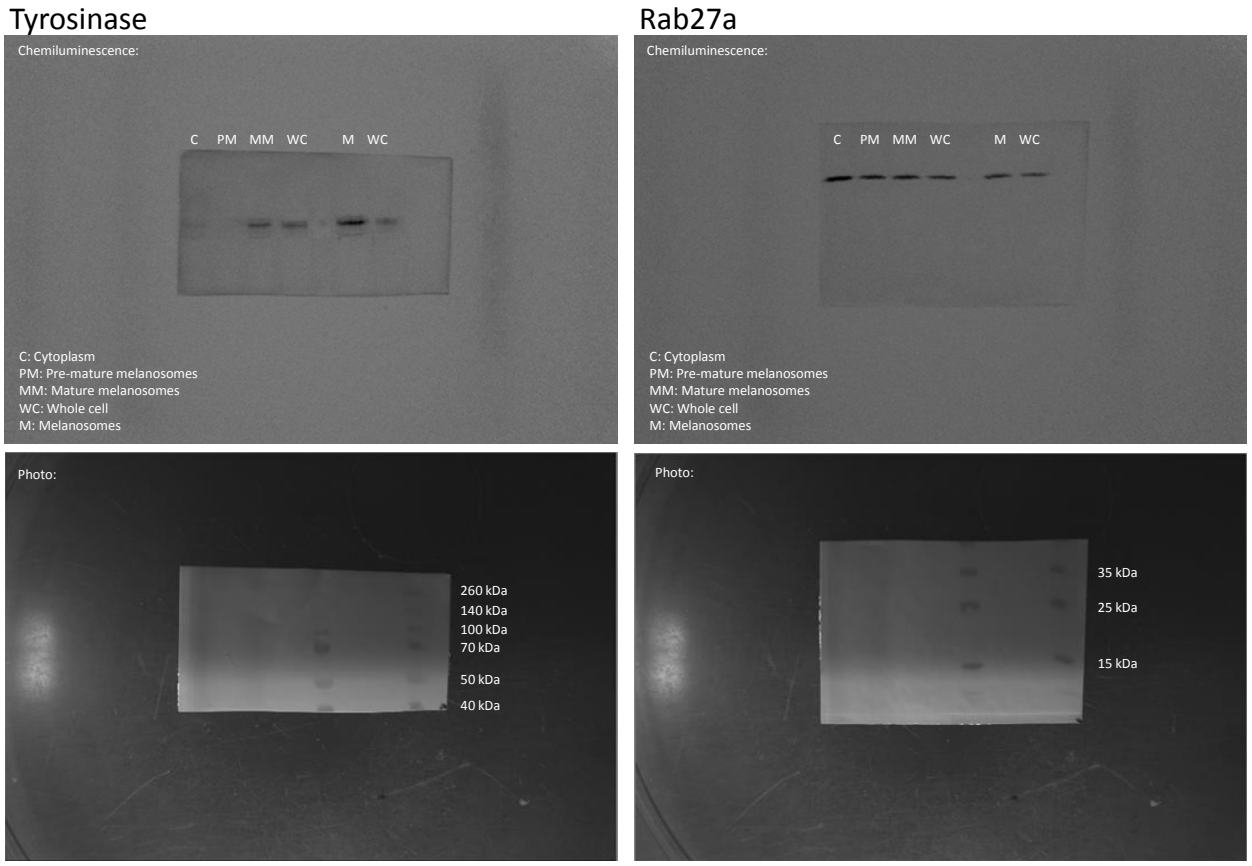

Supplementary Figure 8 Unprocessed scans of western blots

Supplementary Figure 2e:

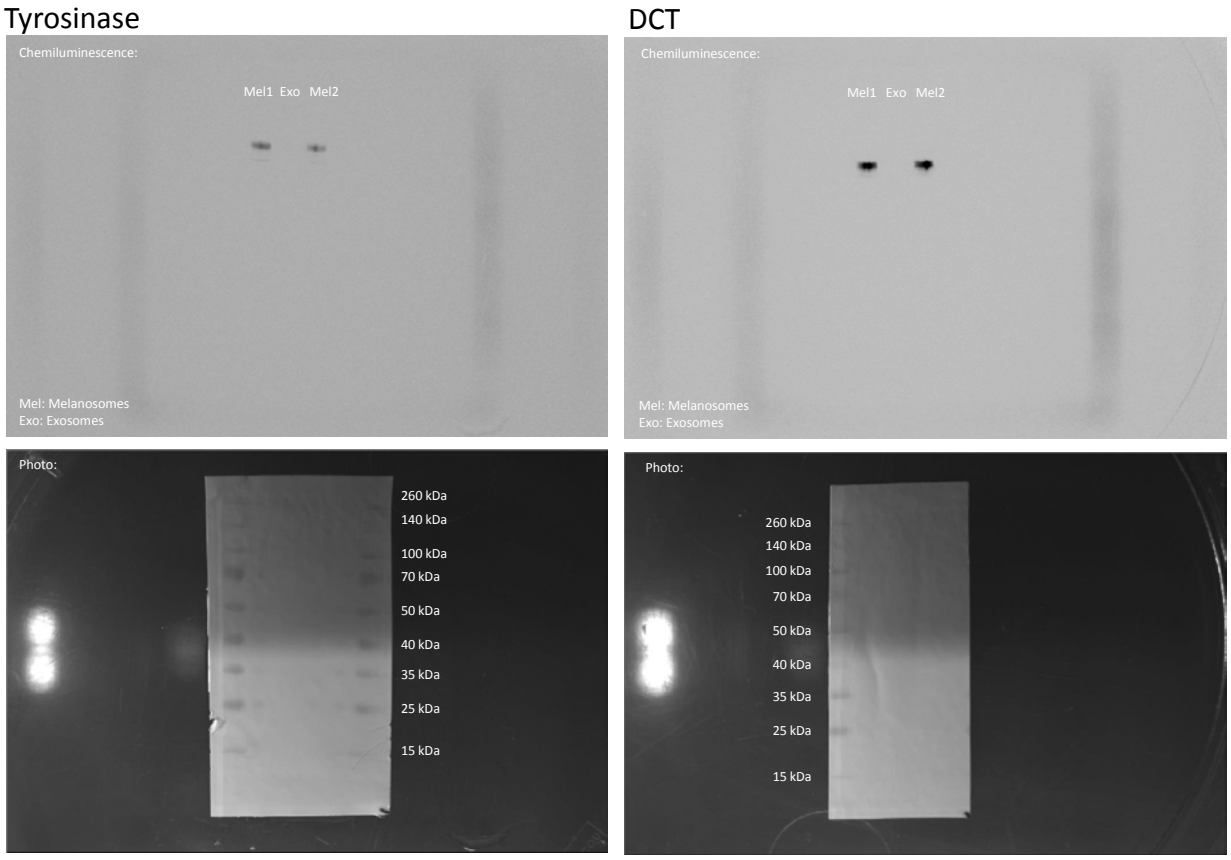

Supplementary Figure 8 continued

Supplementary Figure 2e:

GPNMB

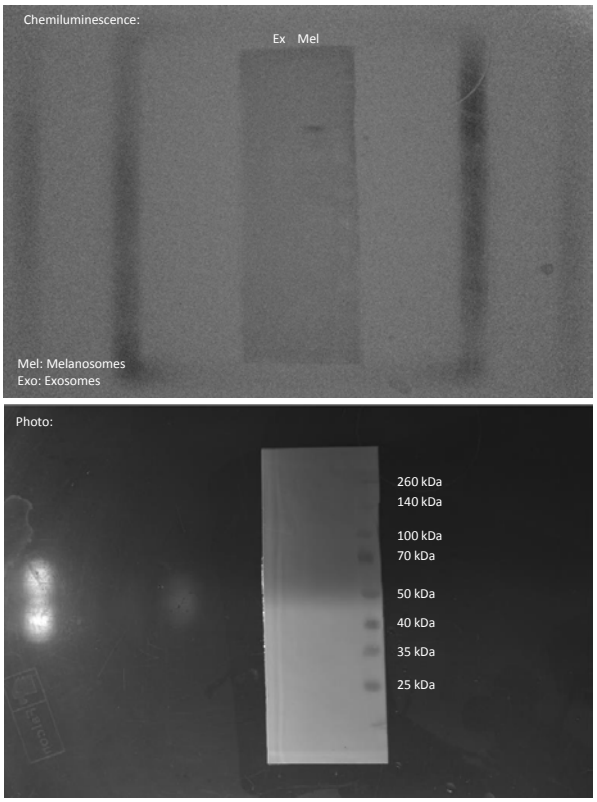

CD63

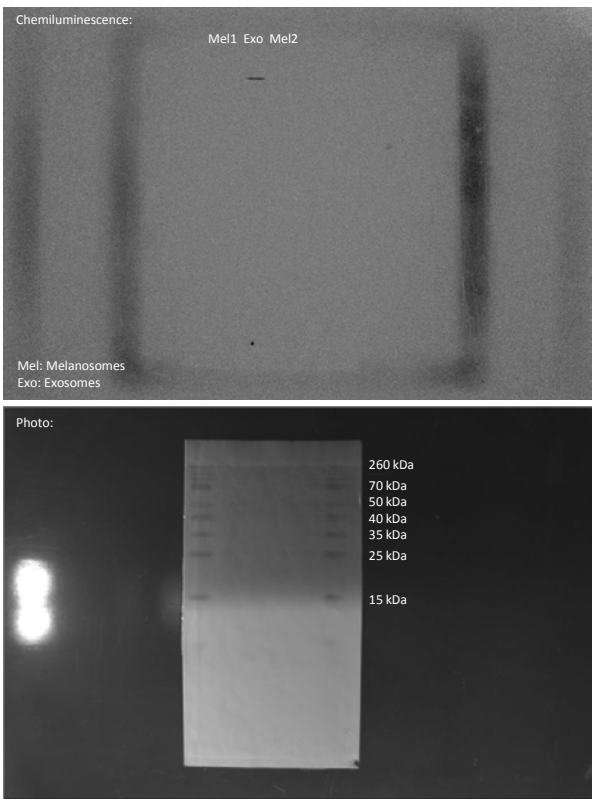

Supplementary Figure 8 continued

Supplementary Figure 2e:

α-Enolase

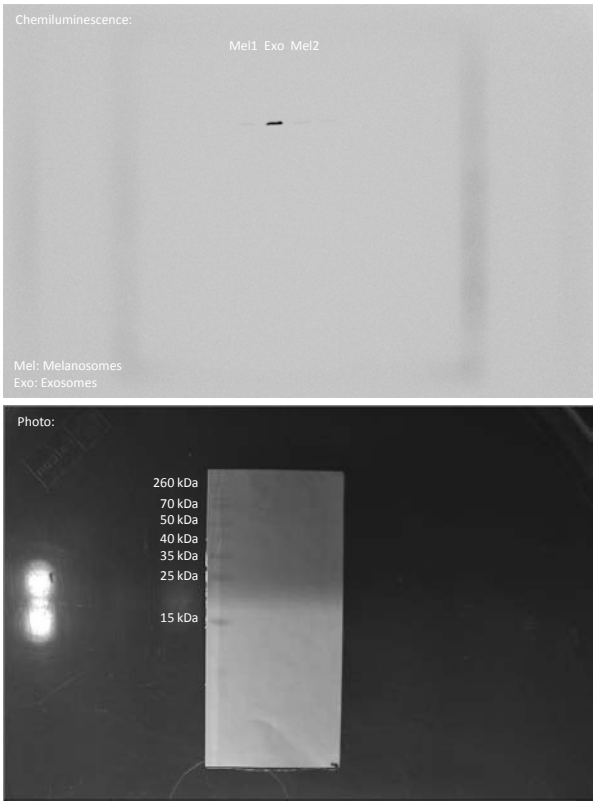

HSC70

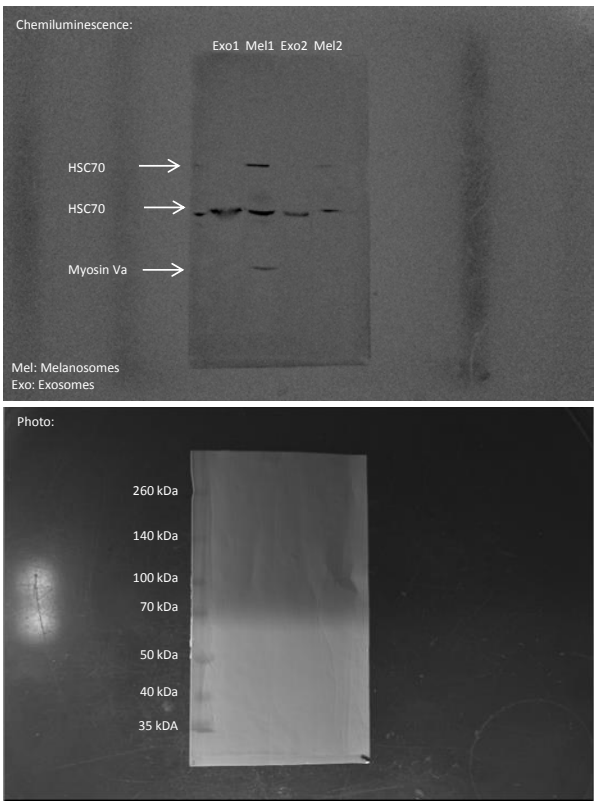

Supplementary Figure 8 continued

Figure 6d

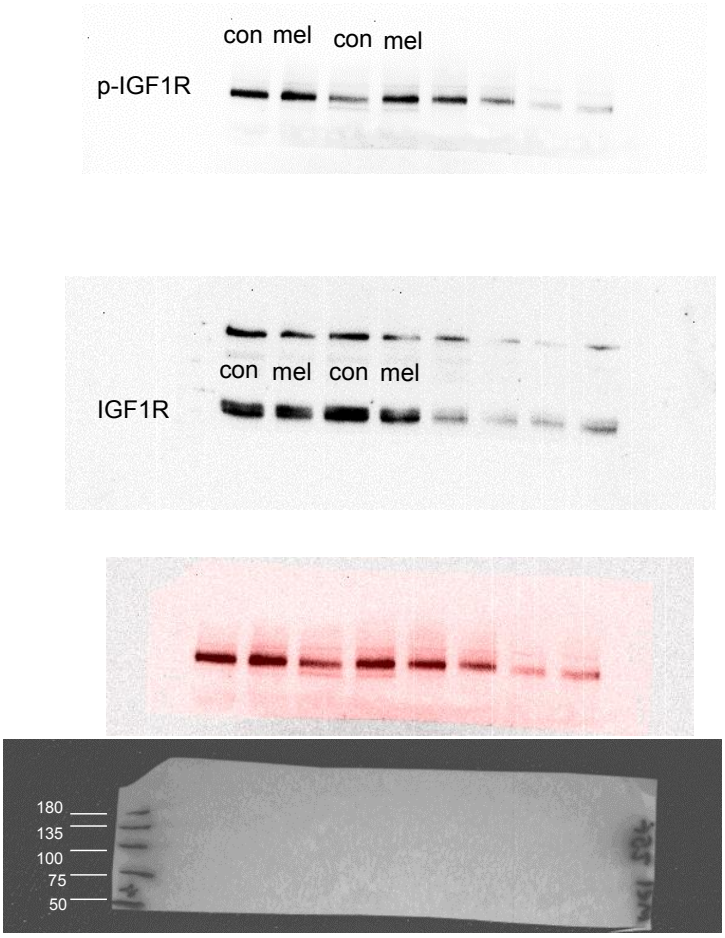

Supplementary Figure 8 continued

Figure 6d

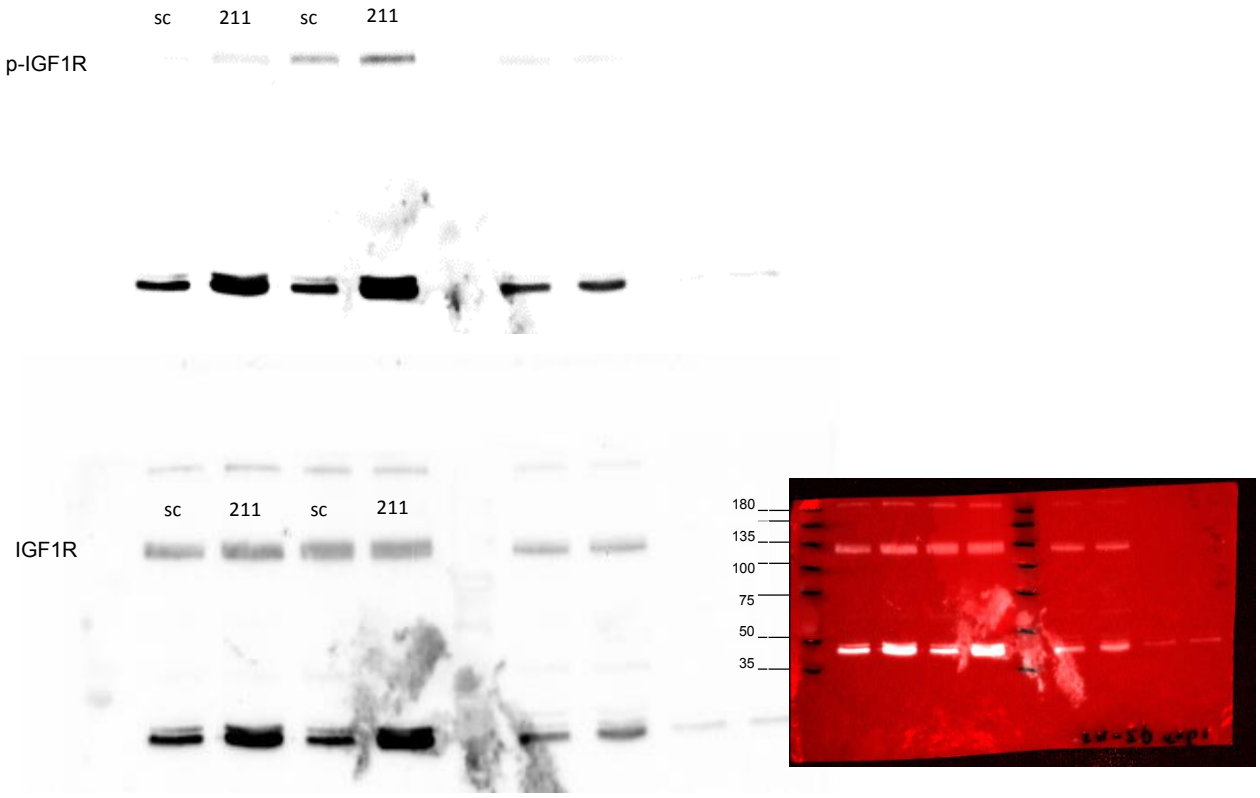

Supplementary Figure 8 continued

Figure 6d

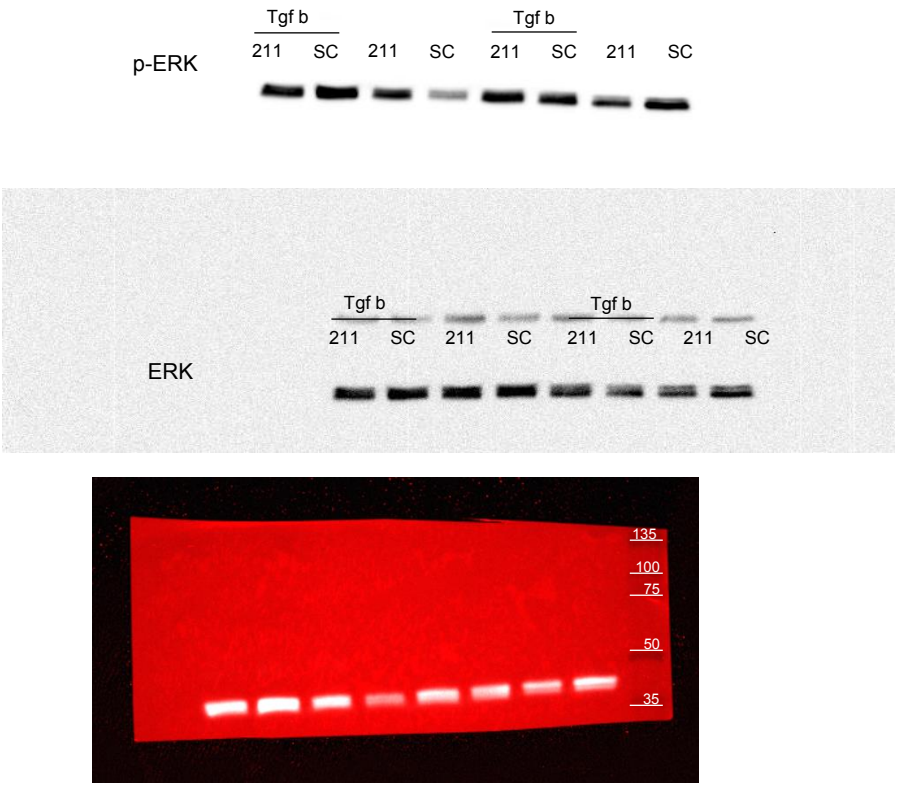

Supplementary Figure 8 continued

Figure 6d

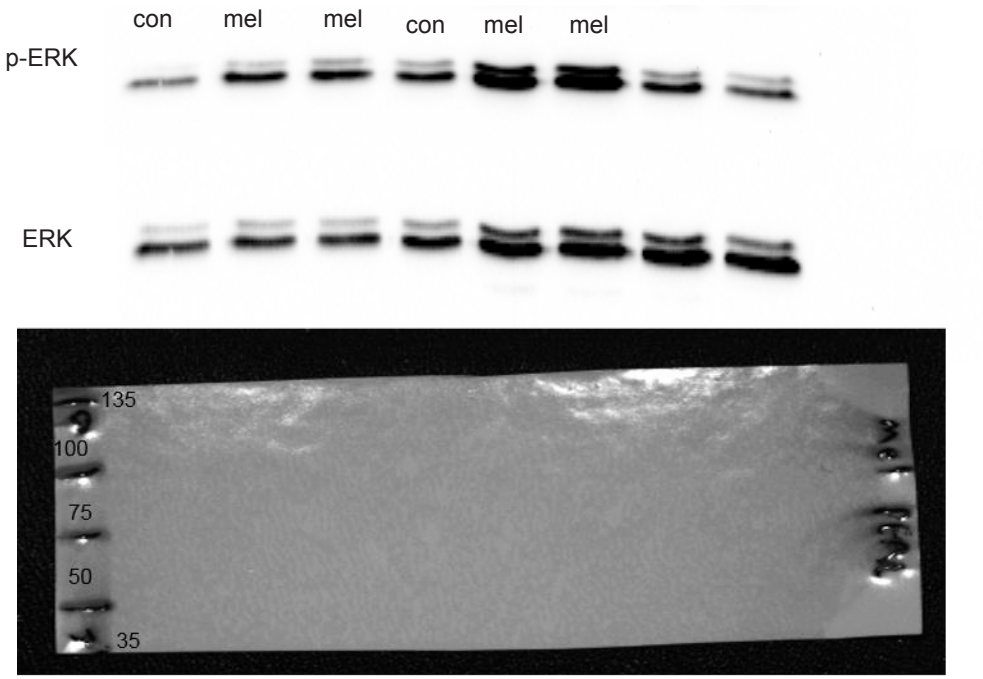

Supplementary Figure 8 continued

Supplementary Figure 6d:

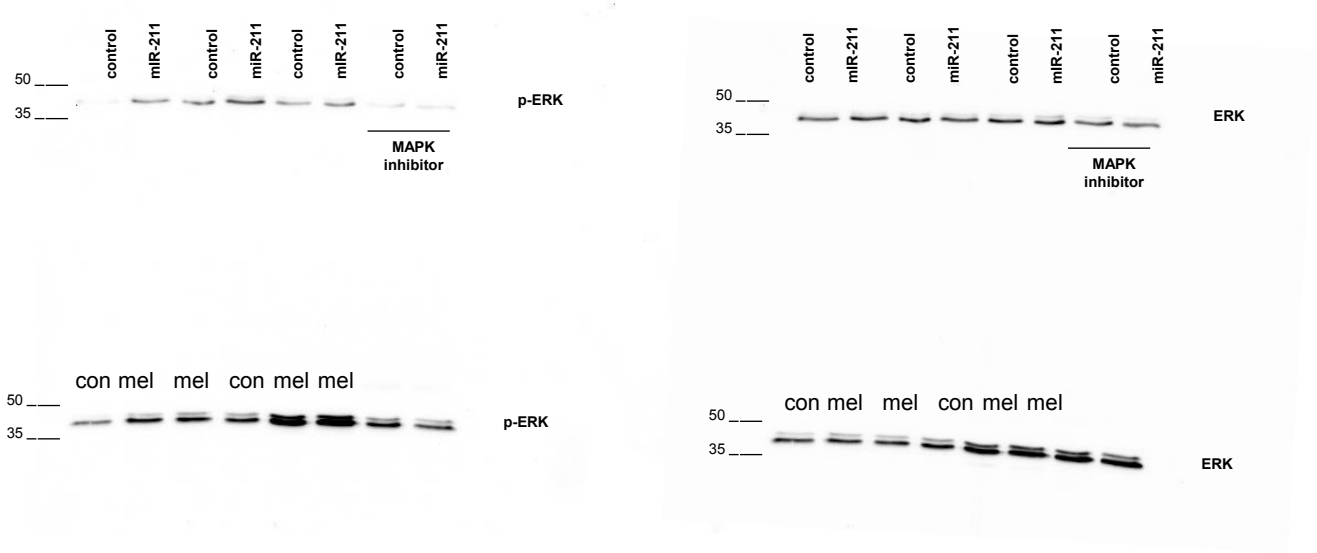

Supplementary Figure 8 continued

Supplementary Figure 6d

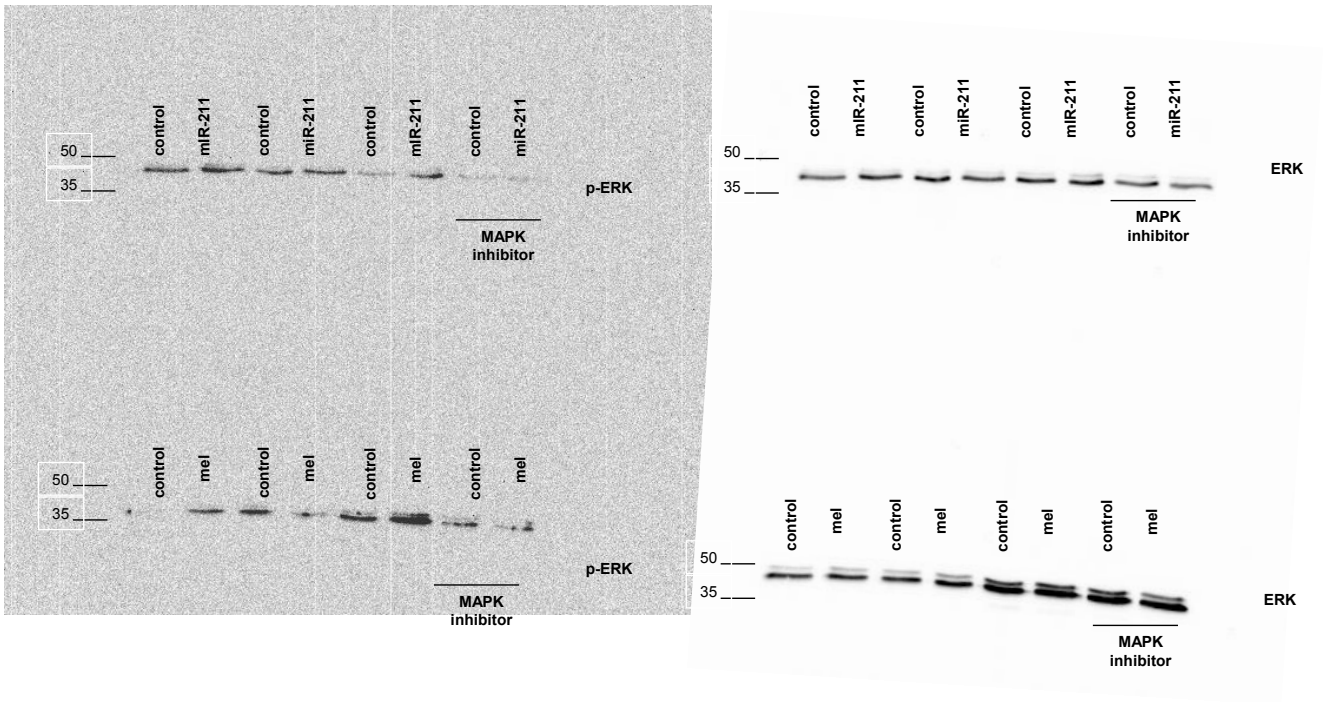

Supplementary Figure 8 continued

Supplementary Table 1 Primary fibroblasts 10%of most differentially expressed mRNA Data Sets

Supplementary Table 2 Ingenuity pathway analysis Data Sets

Supplementary Table 3 miRNA profiling Data Sets

Supplementary Table 4 Overlap of 2000 downregulated mRNA upon miR-211 and melanosomes Data Sets.

Supplementary Table 5 miRNA profiling secreted vesicles Data Sets

Supplementary Table 6 miRNA profiling various melanoma Data Sets

Supplementary Table 7 Oligonucleotides Data Sets

Supplementary Table 8 Statistics Source Data

Supplementary Table 9 Antibodies list

Supplementary Video 1 Isolated liposomes